JCB Journal of Cell Biology

ARTICLE

Cdc5-mediated Ulp2 phosphorylation controls the timing of polySUMOylation during the cell cycle

Emily Gutierrez-Morton[1], Raed Rizkallah[1], Tomiwa Lawal[1], Marie-Helene Kabbaj[1], Sophia L. Owutey[1], Robert J. Tomko Jr[1], and Yanchang Wang[1]

SUMOylation is a posttranslational modification, and polySUMOylation can further trigger protein ubiquitination and relocalization to facilitate cell cycle progression. Previous studies show cell cycle–dependent polySUMOylation in budding yeast, and depletion of SUMO protease Ulp2 causes premature polySUMOylation. Furthermore, Ulp2 undergoes phosphorylation in a manner dependent on mitotic kinase Cdc5. In this study, we report that Cdc5 is necessary for protein polySUMOylation and artificially tethering Cdc5 to Ulp2 is sufficient to trigger polySUMOylation. We further identified serine 734 as the primary phosphorylation site on Ulp2, which is regulated by Cdc5 kinase and Rts1-associated PP2A phosphatase. Notably, phosphodeficient *ulp2*^{S734A} mutant suppressed the polySUMOylation induced by *CDC5* overexpression or *RTS1* deletion. Finally, we found that Ulp2 phosphorylation at serine 734 compromised its binding to SUMO chains. Collectively, these results demonstrate that Cdc5-dependent phosphorylation of SUMO protease Ulp2 reduces its SUMO chain affinity and induces protein polySUMOylation, but PP2A^{Rts1} counteracts this to prevent premature polySUMOylation.

Introduction

SUMOylation is a posttranslational modification that attaches a small ubiquitin-like modifier (SUMO) to target proteins, thereby regulating their subcellular localization, stability, and function (Geiss-Friedlander and Melchior, 2007; Gutierrez-Morton and Wang, 2024). In budding yeast *Saccharomyces cerevisiae*, over 100 SUMO substrates have been identified (Albuquerque et al., 2013; Wohlschlegel et al., 2004), whereas human cells harbor ∼7,000 SUMO-modified proteins (Guerra de Souza et al., 2016; Han et al., 2018). Disruption in SUMO homeostasis is associated with cancers and neurodegenerative diseases (Princz and Tavernarakis, 2020; Xie et al., 2020). Similar to ubiquitination, SUMOylation is mediated through a sequential enzymatic cascade involving an E1-activating enzyme, an E2-conjugating enzyme, and E3 ligases (Capili and Lima, 2007; Kerscher et al., 2006). In budding yeast, the heterodimer Aos1/Uba2 serves as the SUMO E1 enzyme, Ubc9 acts as the sole E2 enzyme, and several E3 ligases—such as Siz1, Siz2, Mms21, and Zip3—catalyze substrate SUMOylation (Johnson and Gupta, 2001; Takahashi et al., 2001; Zhao and Blobel, 2005).

Protein SUMOylation can result in various forms, including mono/non-chain SUMOylation and polySUMOylation (Keiten-Schmitz et al., 2019). PolySUMOylation is the addition of a SUMO chain to a target protein, which has been shown to promote proteasomal turnover of SUMO substrates through the polySUMO axis (Gutierrez-Morton et al., 2024). This polySUMO axis includes SUMO-targeted ubiquitin ligases (STUbLs) that specifically recognize SUMO chains and ubiquitinate polySUMOylated substrates. The Slx5/Slx8 heterodimer is the best-characterized STUbL in budding yeast (Mullen and Brill, 2008; Prudden et al., 2007; Xie et al., 2007). Following STUbL-mediated ubiquitination, substrates are further recognized and extracted by the segregase Cdc48/p97 and subsequently targeted for proteasomal degradation (Bergink et al., 2013; Folger and Wang, 2021). PolySUMOylation plays a crucial role in various cell cycle–regulated cellular processes. For instance, we recently showed how polySUMO-dependent delocalization and degradation of nucleolar protein Tof2 regulate Cdc14 release and mitotic exit (Gutierrez-Morton et al., 2024). Consistently, nucleolar localization of SUMO protease prevents Tof2 degradation (Liang et al., 2017). Moreover, polySUMOylation is implicated in sister chromatid segregation. The cohesin cofactor Pds5 protects the cohesin subunits from polySUMOylation and subsequent disassembly/degradation, thus this process is crucial for maintaining sister chromatid cohesion (D'Ambrosio and Lavoie, 2014; Psakhye and Branzei, 2021). Additionally, the mitotic substrate and nuclease Mus81-Mms4, which is important for maintaining genome stability, undergoes cell cycle–regulated polySUMOylation and degradation (Waizenegger et al., 2020). Overall, these diverse functions highlight the importance of polySUMOylation as a key regulatory mechanism for cell cycle progression.

[1]Department of Biomedical Sciences, College of Medicine, Florida State University, Tallahassee, FL, USA.

Correspondence to Yanchang Wang: yanchang.wang@med.fsu.edu.

https://doi.org/10.1083/jcb.202501146

On the other hand, SUMO proteases reverse SUMOylation by cleaving SUMO moieties from target proteins. In yeast, two SUMO proteases, Ulp1 and Ulp2, perform distinct roles. While both recognize nuclear substrates, Ulp1 localizes at the nuclear pores, and this location could allow Ulp1 to remove SUMO from SUMOylated cargo proteins during their passage through the nuclear pore channel (Panse et al., 2003). Disruption of Ulp1 localization at nuclear periphery results in broad protein deSUMOylation (de Albuquerque et al., 2016). In contrast, Ulp2 localizes in the nucleus and plays a critical role in disassembling polySUMO chains by cleaving them from their distal ends, typically reducing the chains to one or two SUMO moieties on the target protein (Eckhoff and Dohmen, 2015; Kramarz et al., 2020; Li and Hochstrasser, 2003; Mossessova and Lima, 2000). Therefore, Ulp2 likely prevents polySUMOylation of nuclear proteins. Ulp2 contains a C-terminal SUMO-interacting motif (SIM) (Li and Hochstrasser, 2000), comprised of a core consensus of I/V-X-I/V-I/V with an acidic residue typically flanking one side of the motif (Song et al., 2004). The Ulp2 SIM, located between amino acids 725 and 728, is critical for its ability to bind and cleave polySUMO chains (de Albuquerque et al., 2018). The electrostatic interactions between SUMO and SIM exhibit relatively modest binding affinity (Song et al., 2004). Notably, *in vitro* data show that Ulp2 binds weakly to monomeric SUMO but has a stronger affinity for extended SUMO chains, which is consistent with its role in cleaving SUMO chains (de Albuquerque et al., 2018). Furthermore, *in vivo* data reveal that Ulp2-mediated deSUMOylation of substrates, such as Tof2, depends on the SIM (de Albuquerque et al., 2018). This raises the intriguing possibility that the SUMO chains on target proteins act as recruitment signals for Ulp2, facilitating their own cleavage to prevent polySUMOylation. Indeed, we recently found that nuclear depletion of Ulp2 triggers protein polySUMOylation (Gutierrez-Morton et al., 2024).

PolySUMOylation is tightly regulated during the cell cycle, with many substrates undergoing polySUMO-dependent turnover during anaphase entry (Gutierrez-Morton et al., 2024). However, the molecular switch between non-chain SUMOylation and polySUMOylation during the cell cycle remains unknown. Previous work shows that Ulp2 is negatively regulated by Cdc5 kinase through phosphorylation during mitosis (Baldwin et al., 2009). Cdc5 kinase is the single polo-like kinase found in budding yeast, and its activity is crucial for coordinating mitotic events, such as chromosome segregation and condensation, as well as mitotic exit (Alexandru et al., 2001; Hu et al., 2001; St-Pierre et al., 2009). Cdc5 is believed to regulate Ulp2 activity by mediating phosphorylation at its C-terminal domain (Baldwin et al., 2009). An attractive hypothesis is that Cdc5-dependent Ulp2 phosphorylation reduces Ulp2's SUMO chain cleavage activity, which leads to the switch to polySUMOylation. However, the specific molecular mechanisms underlying this regulation, including the phosphorylation sites on Ulp2 and the biological significance of this modification, remain elusive.

In this study, we investigated the molecular mechanism that controls the timing of protein polySUMOylation during the cell cycle in budding yeast. We previously showed that nucleolar protein Tof2 undergoes polySUMO-dependent delocalization and degradation to facilitate mitotic exit (Gutierrez-Morton et al., 2024). Here, we first demonstrate that *cdc5* mutant cells exhibit reduced accumulation of polySUMO conjugates, including Tof2, as well as impaired Tof2 delocalization and degradation during the cell cycle. In contrast, Cdc5 overexpression is sufficient to trigger global polySUMOylation as well as polySUMO-dependent Tof2 delocalization and turnover. Remarkably, the induced binding of Cdc5 to Ulp2 can also trigger polySUMOylation and polySUMO-mediated processes. We further provide evidence that Cdc5 promotes Ulp2 phosphorylation at serine 734 (S734) to negatively regulate Ulp2's enzyme activity. Additionally, we show that Rts1-associated protein phosphatase 2A (PP2A) phosphatase prevents premature Ulp2 phosphorylation. Finally, we demonstrate that Ulp2 phosphorylation at S734 reduces its affinity for SUMO chains. Overall, our findings support the conclusion that Cdc5-dependent phosphorylation of the SUMO protease Ulp2 downregulates Ulp2 by reducing its SUMO chain binding, thereby promoting protein polySUMOylation. However, $PP2A^{Rts1}$ counteracts this modification to prevent premature polySUMOylation, thereby revealing the molecular mechanisms that control the timing of polySUMOylation during the cell cycle.

Results

Cdc5 kinase facilitates protein polySUMOylation in budding yeast

We recently demonstrated that protein polySUMOylation is cell cycle regulated, and polySUMOylated conjugates disappear concurrently with anaphase inhibitor Pds1. Additionally, a nucleolar anchor of Cdc14 phosphatase, Tof2, undergoes polySUMO-dependent delocalization and degradation, leading to partial Cdc14 release and mitotic exit (Gutierrez-Morton et al., 2024). Therefore, Tof2 is an ideal substrate to investigate the regulation of protein polySUMOylation. *cdc5* mutants exhibit reduced SUMO conjugates (Baldwin et al., 2009), but whether this is a result of defective SUMOylation or polySUMOylation remains unclear. To clarify this issue, we analyzed both overall SUMOylation and Tof2 SUMOylation in *cdc5-2* cells, which arrest in anaphase at the restrictive temperature (Hu et al., 2001). We included *cdc15-2* mutant as a control, as it also shows telophase arrest with active Cdc5 at high temperatures (Liang et al., 2009; Surana et al., 1993). Since the *SMT3* gene encodes the sole SUMO protein in budding yeast, we used yeast strains with chromosomally expressed His-FLAG-Smt3 (HF-Smt3) to examine protein SUMOylation (Ohkuni et al., 2016). G_1-arrested *cdc5-2* and *cdc15-2* cells with HF-Smt3 and Tof2-13myc were released into 36°C for 2 h to induce cell cycle arrest, after which cell lysates were prepared. Following immunoprecipitation (IP) of HF-Smt3 for SUMOylated protein species with an anti-FLAG antibody, we assessed both overall SUMOylation and Tof2 SUMOylation in these cells. SUMOylation was detected in both *cdc5-2* and *cdc15-2* mutants, but the latter exhibited slightly reduced overall SUMOylation and Tof2 SUMOylation (Fig. 1 A, lanes 2 and 4). One explanation is that polySUMO-dependent degradation contributes to the reduced level of SUMOylated proteins in *cdc15-2* cells.

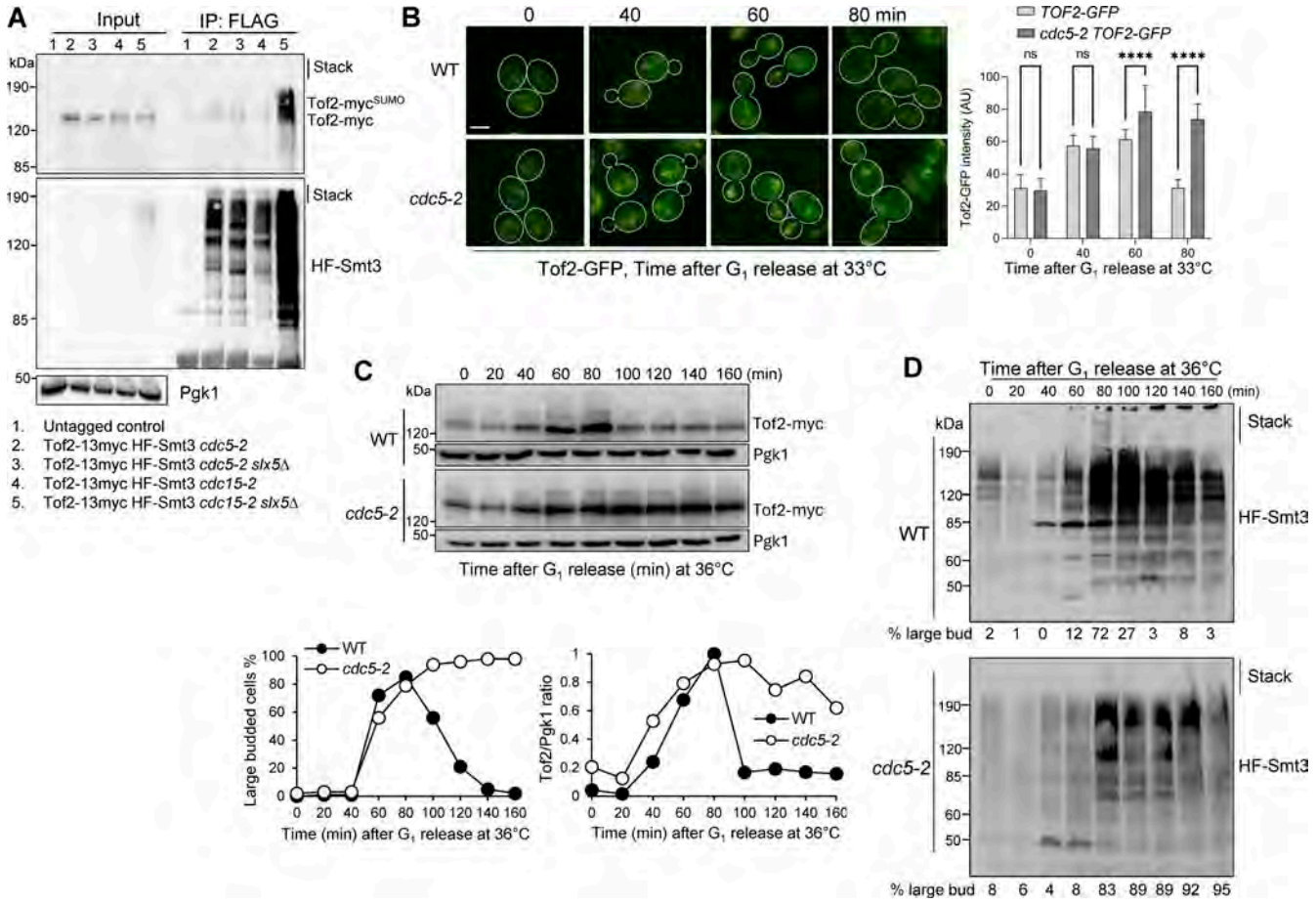

Figure 1. **Cdc5 kinase governs polySUMOylation during the cell cycle. (A)** The *cdc5-2* mutant shows defective polySUMO-dependent Tof2 degradation. Untagged control (Y300), 4922-3-4 (*cdc5-2*), 4944-1-3 (*cdc5-2 slx5Δ*), 4920-2-1 (*cdc15-2*), and 5030-2-2 (*cdc15-2 slx5Δ*) cells expressing HF-Smt3/SUMO and Tof2-13myc were grown to mid-log phase at 25°C. The cells were first arrested in G_1 phase with α-factor and then released to 36°C for 2 h for *cdc5-2/cdc15-2* arrest. Cell extracts were prepared and immunoprecipitated (IPed) to precipitate HF-Smt3/SUMO conjugates. HF-Smt3 and Tof2-13myc protein levels in the input and IPed fraction were detected by western blotting with anti-FLAG and anti-myc antibodies. Pgk1, loading control. **(B)** Tof2-GFP nucleolar delocalization is dependent on Cdc5 activity. G_1-arrested *TOF2-GFP* (EGM3) and *cdc5-2 TOF2-GFP* (4802-4-1) cells at 25°C were released into 33°C YPD for Cdc5 inactivation, and time points were taken to examine Tof2-GFP intensity. Representative images of Tof2-GFP in these synchronized cells are shown. Scale bar, 5 µm. The average Tof2-GFP intensity for each time point (n = 50 cells) was quantified. Statistical analysis used two-way ANOVA with Tukey's test. The bar graph represents mean values ± SD. **** $p < 0.0001$. **(C)** Cell cycle–dependent turnover of Tof2 is prevented in *cdc5-2* cells. G_1-arrested WT (YYW273) and *cdc5-2* (4123-2-3) cells with Tof2-13myc at 25°C were released into the cell cycle at 36°C. Cells were collected every 20 min for western blotting (top) and budding index (bottom left). Pgk1, loading control. The bottom right graph is the ratio of Tof2 to Pgk1 protein levels during the cell cycle. **(D)** Decreased accumulation of polySUMOylated conjugates in *cdc5-2* mutants during the cell cycle. G_1-arrested WT (4160-1-2) and *cdc5-2* (4161-3-2) cells with HF-Smt3 at 25°C were released into the cell cycle at 36°C. Cells were collected every 20 min for budding index (bottom) and western blotting with anti-FLAG antibody. Source data are available for this figure: SourceData F1.

Slx5 is a subunit of STUbL that catalyzes polySUMO-mediated protein ubiquitination for the subsequent segregation by the Cdc48 complex and degradation by proteasomes. Thus, we introduced *slx5Δ* to *cdc5-2* and *cdc15-2* mutants to stabilize SUMO substrates including Tof2. Strikingly, *slx5Δ* mutation significantly increased the levels of both overall SUMOylation and Tof2 SUMOylation in *cdc15-2* cells but had no effect on *cdc5-2* mutants. In addition, much more polySUMOylated Tof2 was detected in *cdc15-2 slx5Δ* cells (Fig. 1 A, lanes 3 and 5). Therefore, comparisons of Tof2 SUMOylation in *cdc5-2* and *cdc15-2* arrested cells with and without *slx5Δ* supports a model in which Cdc5 kinase activity facilitates polySUMOylation.

Tof2 undergoes polySUMO-dependent relocalization and turnover during the cell cycle (Gutierrez-Morton et al., 2024). To determine whether *cdc5-2* mutation disrupts this process, we monitored Tof2-GFP localization throughout the cell cycle after G_1 release. In WT cells, Tof2-GFP displayed a characteristic increase in GFP fluorescence intensity at the nucleolus after G_1 release with peaking at 60 min, followed by nucleolar delocalization and a decline in GFP intensity (Fig. 1 B). In contrast, *cdc5-2* mutants exhibited stable nucleolar fluorescence intensity of Tof2. Consistently, *cdc5-2* mutants also showed stabilized Tof2-myc protein level during cell cycle compared with WT cells (Fig. 1 C), supporting the role of Cdc5 in facilitating polySUMO-mediated Tof2 nucleolar delocalization and degradation. We next examined total protein SUMOylation during the cell cycle in WT and *cdc5-2* mutants expressing HF-Smt3 (Fig. 1 D). In WT cells, polySUMOylation exhibited clear cell cycle regulation,

peaking at 80 min, with high–molecular weight polySUMOylated species becoming trapped in the stacking gel. However, *cdc5-2* mutants showed much less signal in the stacking gel. We also noticed a reduced level of SUMO conjugates in *cdc5-2* mutant cells, and the level was relatively consistent after 80 min. We speculate that the reduced polySUMOylation in *cdc5-2* mutants likely contributes to both the low level of SUMO conjugates and their stabilization. Together, these results suggest that Cdc5 promotes polySUMOylation and its downstream processes.

Cdc5 overexpression triggers polySUMO-dependent Tof2 nucleolar release and degradation

If Cdc5 kinase promotes polySUMOylation, Cdc5 overproduction is expected to increase the level of polySUMOylation. To test this idea, we transformed yeast cells with P_{GAL}*CDC5* plasmids, in which the *CDC5* gene is under the control of a galactose-inducible promoter (*GAL*) (Hu et al., 2001). We then assessed the impact of Cdc5 overproduction on Tof2 SUMOylation (Fig. 2 A). To rule out interference from endogenous Cdc5 expression, which begins during late S phase (Charles et al., 1998), we conducted experiments in cells arrested in S phase with hydroxyurea (HU), a DNA synthesis inhibitor, so that endogenous Cdc5 expression and activity remain minimal. Additionally, cells were treated with proteasome inhibitor MG-132 to block proteasomal degradation of Tof2 and other substrates. The results of HF-Smt3 IP revealed that cells arrested either in G_1 or S phase showed reduced, yet detectable, Tof2 SUMOylation. In contrast, a more significant accumulation of polySUMOylated conjugates, including Tof2, was detected following Cdc5 overexpression, consistent with the positive role of Cdc5 kinase in polySUMOylation.

Since Cdc5 overexpression induced Tof2 polySUMOylation, we next investigated whether it also impacts Tof2 localization and protein stability. In Fig. 2 B, *NET1-GFP TOF2-mApple* yeast cells with vector or P_{GAL}*CDC5* were grown in raffinose media to log phase and then arrested with HU before galactose was added to induce Cdc5 overproduction. Compared with cells with vector control, cells overproducing Cdc5 showed a significant decrease in Tof2-mApple intensity. Nucleolar protein Net1 plays a major role in mitotic exit by anchoring Cdc14 phosphatase (Shou et al., 1999; Shou et al., 2002; Visintin et al., 1999). Although Net1 is also a SUMO target, unlike Tof2, it does not undergo polySUMO-dependent nucleolar release and degradation (Gutierrez-Morton et al., 2024; Liang et al., 2017). In contrast to Tof2-mApple, the Net1-GFP signal was minimally affected (Fig. 2 B). Tof2 also underwent significant protein turnover following Cdc5 overexpression (Fig. 2 C). Strikingly, this turnover was blocked in *smt3-KRall* cells, where all lysine residues in SUMO (Smt3) were mutated to arginine, thereby preventing SUMO chain formation (Bylebyl et al., 2003; Psakhye et al., 2019). We also used *smt3-KRall* mutant to determine whether the loss of Tof2 intensity after Cdc5 overproduction was polySUMO-dependent. In cells overproducing Cdc5, the introduction of *smt3-KRall* mutant prevented the loss of Tof2-GFP signal intensity (Fig. 2 D). Together, these results indicate that Cdc5 overexpression triggers polySUMO-mediated Tof2 nucleolar delocalization and degradation.

Tethering Cdc5 to Ulp2 is sufficient to induce polySUMOylation

Our recent work indicates that SUMO protease Ulp2 prevents polySUMOylation (Gutierrez-Morton et al., 2024). Ulp2 interacts with Cdc5 kinase and undergoes phosphorylation during mitosis in a Cdc5-dependent manner (Baldwin et al., 2009; Snead et al., 2007; Srikumar et al., 2013). We speculated that Cdc5 promotes Ulp2 phosphorylation to compromise its protease activity. Therefore, we examined the effect of enforced Cdc5–Ulp2 interaction on polySUMOylation. For this purpose, we generated an inducible artificial tethering system to temporally control Cdc5–Ulp2 interaction. The tethering system uses GFP-binding protein (GBP), a nanobody fragment with high GFP affinity (Rothbauer et al., 2006; Rothbauer et al., 2008). We demonstrated the colocalization of GBP with GFP-tagged proteins in yeast cells (Folger et al., 2025). As shown in Fig. 3 A, we first constructed a P_{DDI2}*HA-GBP-CDC5* plasmid, where HA-GBP-Cdc5 expression is under the control of a *DDI2* promoter, which is induced by cyanamide (Lin et al., 2018). We then introduced the P_{DDI2}*HA-GBP-CDC5* plasmid into yeast strains expressing Ulp2-GFP, which enabled us to induce the tethering of Cdc5 to Ulp2. Yeast cells with Ulp2-GFP and P_{DDI2}*HA-GBP-CDC5* were arrested in S phase with HU to prevent expression of endogenous Cdc5, and then HA-GBP-Cdc5 expression was induced by cyanamide. Total SUMOylation levels increased over time after HA-GBP-Cdc5 induction (Fig. 3 B, left panel). Notably, the levels of high–molecular weight polySUMOylated species were relatively high in the stacking gel at 30 and 60 min but decreased slightly by 90 min, likely due to the degradation of polySUMOylated proteins. We also performed this experiment in the STUbL mutant *slx5Δ* after induction of Cdc5–Ulp2 interaction, since *slx5Δ* stabilizes polySUMOylated proteins by blocking polySUMO-dependent ubiquitination. As expected, following forced Cdc5–Ulp2 interaction, we observed significantly increased levels of SUMOylated protein species, including those with high–molecular weight (Fig. 3 B, middle left panel). In contrast, forced tethering of $Cdc5^{KD}$, a kinase-dead Cdc5 (N209A mutation) (Bartholomew et al., 2001), to Ulp2 did not cause a pronounced increase in total polySUMOylation levels, even in *slx5Δ* cells (Fig. 3 B, right two panels). Based on these observations, we conclude that enforced Cdc5–Ulp2 interaction triggers protein polySUMOylation, and Cdc5 kinase activity is required for this process.

We next investigated whether induced Cdc5–Ulp2 interaction could trigger untimely Tof2 delocalization and degradation. Cells expressing Tof2-mApple and Ulp2-GFP were transformed with the P_{DDI2}*HA-GBP-CDC5/cdc5*^{KD} plasmids. After arresting cells in HU, we induced either GBP-Cdc5 or GBP-$Cdc5^{KD}$ expression by adding cyanamide and measured Tof2 fluorescence intensity after 1 h. As seen in Fig. 3 C, a significant decrease in Tof2 intensity was observed following GBP-Cdc5 expression. This loss likely depends on the polySUMO axis since blocking STUbL activity in *slx5Δ* mutant restored Tof2 fluorescence intensity. Additionally, the expression of $Cdc5^{KD}$ did not lead to a reduction in Tof2 signal. Similarly, Tof2 protein level reduced following induced Cdc5–Ulp2 interaction, and this reduction was blocked by *slx5Δ* mutation (Fig. 3 D). To exclude the possibility that GBP-Cdc5 expression alone induces Tof2

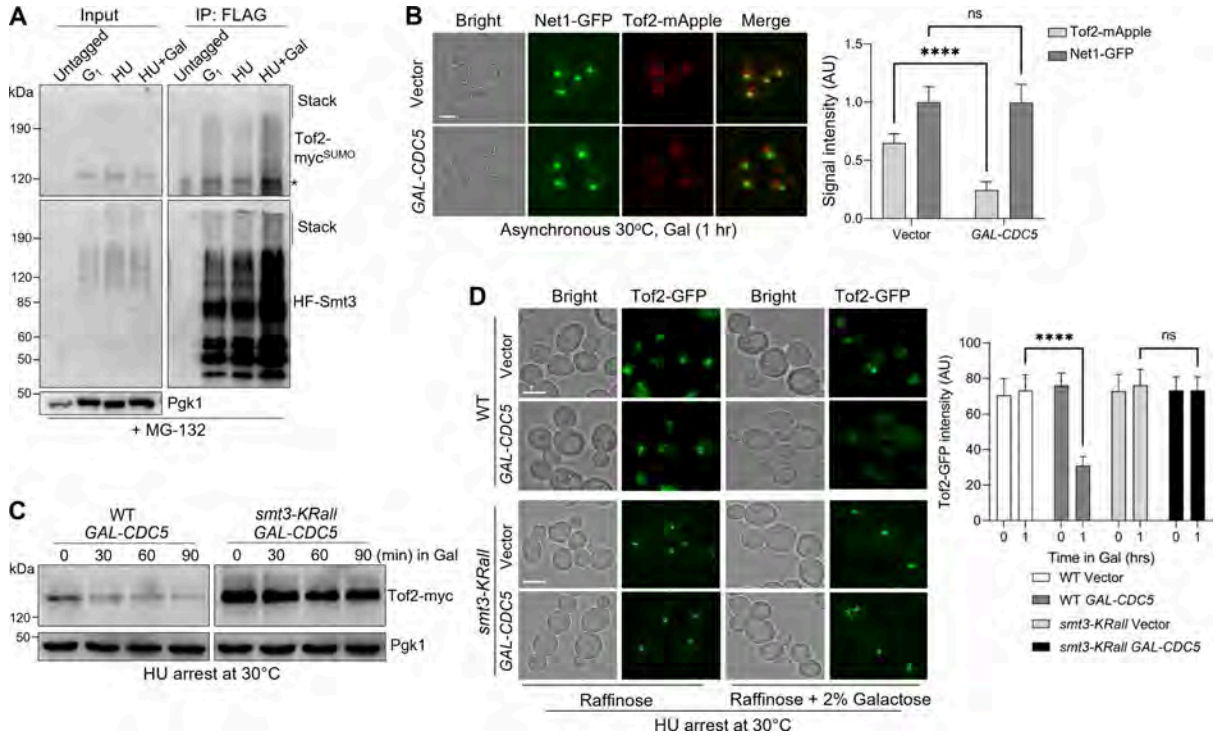

Figure 2. **Overexpression of *CDC5* triggers polySUMO-dependent Tof2 nucleolar release and degradation. (A)** *CDC5* overexpression induces Tof2 polySUMOylation. Cells (4289-3-2) with HF-Smt3, Tof2-13myc, and P_{GAL}*CDC5* plasmid (pFH2) were cultured in -TRP media with 2% raffinose. Cells were arrested in either G_1 by α factor or S phase by 200 mM HU at 30°C for 2 h followed by the treatment with proteasome inhibitor MG-132 for 30 min. Galactose (2%) was then added to HU-arrested cells to induce *CDC5* overexpression for 2 h. Cell extracts were prepared and IPed with anti-FLAG antibody to isolate HF-Smt3 conjugates. HF-Smt3 and Tof2-13myc protein levels in the input and IPed fraction were detected by western blotting with anti-FLAG and anti-myc antibodies. Y300 (untagged) cells served as a negative control. Pgk1, loading control. * denotes nonspecific binding. **(B)** Cdc5 overproduction promotes the nucleolar release of Tof2, but not its paralog Net1. Asynchronous 4255-2-2 cells (*NET1-GFP TOF2-mApple*) containing either P_{GAL}*CDC5* (pFH2) or vector control (pBAD104) in raffinose media were treated with galactose (2%) for 1 h at 30°C for imaging. Scale bar, 5 µm. The average Tof2 and Net1 intensity (n = 50 cells) were quantified. Statistical analysis used two-way ANOVA with Tukey's test. The bar graph represents mean values ± SD. **** $p < 0.0001$. **(C)** *CDC5* overexpression triggers polySUMO-dependent proteasomal degradation of Tof2. HU-arrested WT (YYW273) and SUMO chainless *smt3-KRall* (4914-1-3) cells with Tof2-13myc and pFH2 plasmid in raffinose media were treated with galactose (2%) to induce Cdc5 overproduction at 30°C. Cells were collected every 30 min for the detection of Tof2-13myc protein levels with anti-myc antibody. Pgk1, loading control. **(D)** *CDC5* overexpression reduces Tof2-GFP signal, which is blocked in *smt3-KRall* mutant. *TOF2-GFP* (EGM43) and *TOF2-GFP smt3-KRall* (4799-1-3) cells containing either pFH2 or control vector (pBAD104) were arrested in HU for 2 h at 30°C in -TRP dropout media with raffinose before the addition of galactose (2%) to induce Cdc5 overproduction. Cells were collected before and after galactose induction (1 h) to examine Tof2-GFP intensity. Scale bar, 5 µm. The average Tof2-GFP intensity for each time point (n = 50 cells) was quantified. Statistical analysis used two-way ANOVA with Tukey's test. Bar graph represents mean values ± SD. **** $p < 0.0001$. Source data are available for this figure: SourceData F2. IPed, immunoprecipitated.

degradation, we induced GBP-Cdc5 expression in cells lacking Ulp2-GFP and observed no Tof2 degradation. Moreover, the expression of GBP-Cdc5^{KD} in cells with or without *slx5Δ* mutation did not induce Tof2 degradation. Overall, these results support the conclusion that enforced interaction of Cdc5 kinase and Ulp2 induces polySUMOylation and the untimely degradation of SUMO substrate Tof2. We acknowledge that the GBP system may induce artificial interactions between proteins, and its irreversible binding limits temporal control. In this study, however, the expression of GBP-Cdc5 under the control of a *DDI2* promoter is induced by the addition of cyanamide; its induction is not physiological. Moreover, including GBP-Cdc5^{KD} as a negative control helps clarify the effect of GBP-Cdc5 expression.

Ulp2 S734 is likely the primary phosphorylation site regulated by Cdc5 kinase

Although previous evidence indicates that Cdc5 is required for the phosphorylation of the C-terminal region of Ulp2 (Baldwin et al., 2009), the phosphorylation sites remain to be determined. We first conducted an *in vitro* kinase assay using Ulp2 and Cdc5 proteins purified from bacteria, confirming that incubation with Cdc5 caused Ulp2 band shift (Fig. 4 A). In addition, this band shift was abolished after phosphatase treatment (Fig. 4 B). We next utilized the polo-like kinase 1 phosphorylation consensus sequence (E/D-X-S/T-I/V/L/M/P-X-E/D) (Nakajima et al., 2003) and Group-based Prediction System 6.0 for site prediction (Chen et al., 2023). This analysis revealed four potential phosphorylation sites within the C terminus of Ulp2: S734, S735, S929, and T949. Using CRISPR genome editing (Laughery and Wyrick, 2019), we then generated four yeast *ulp2* alanine substitution mutants, each targeting one of these residues, and analyzed the Ulp2 band shift. Since Ulp2 phosphorylation accumulates in mitosis (Baldwin et al., 2009), we examined the extent of Ulp2 phosphorylation in cells arrested in metaphase with nocodazole. Ulp2 mutants *S929A*, *S735A*, and *T949A* showed phosphorylation patterns similar to those observed in WT. Strikingly, decreased

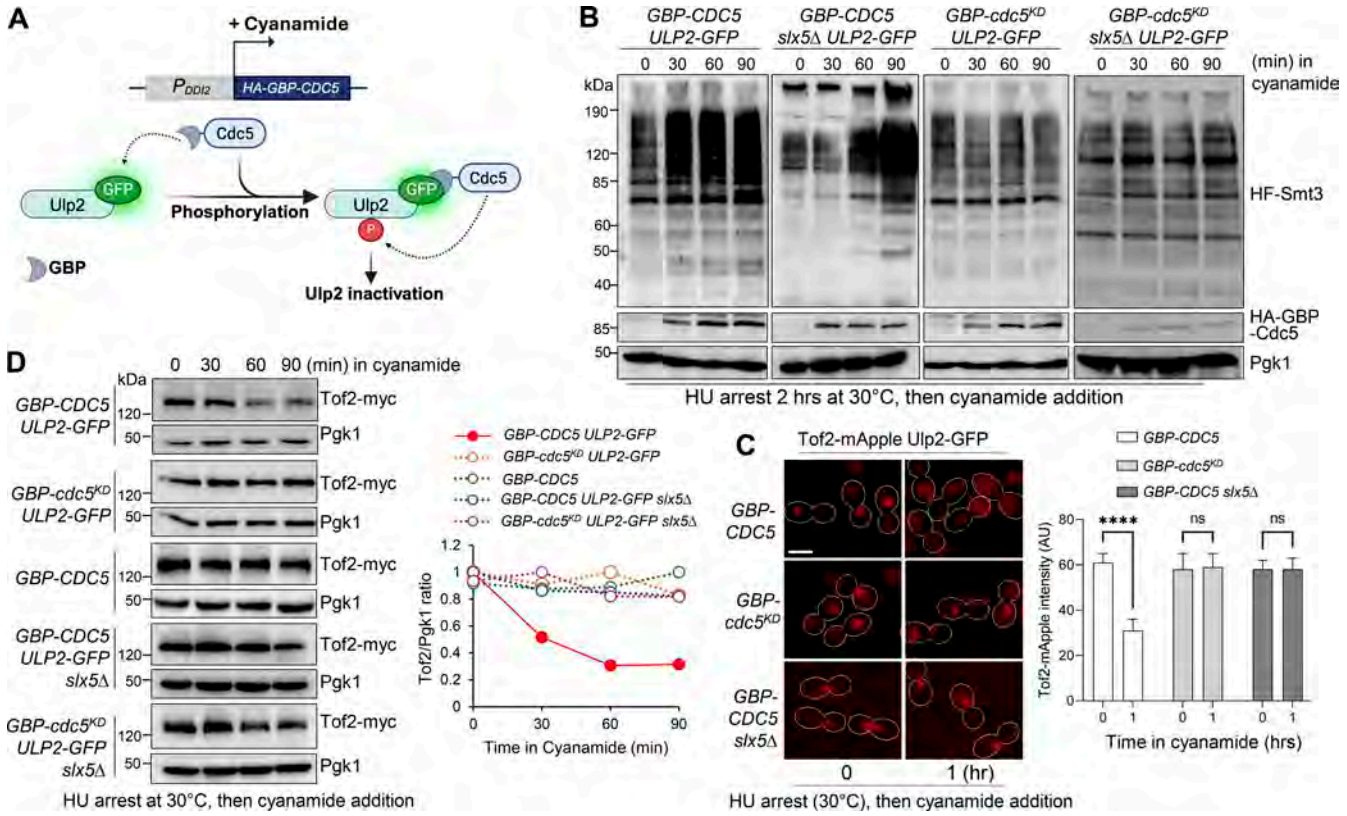

Figure 3. **Tethering Cdc5 kinase to Ulp2 promotes polySUMOylation. (A)** Scheme of the inducible GBP system. HA-GBP-Cdc5 fusion is expressed under the control of a *DDI2* promoter. Induction of HA-GBP-Cdc5 expression by cyanamide results in the recruitment of HA-GBP-Cdc5 to Ulp2-GFP, which is expected to trigger Cdc5-dependent Ulp2 phosphorylation. **(B)** Tethering Cdc5 to Ulp2 induces premature polySUMOylation. Cells with a combination of Ulp2-GFP HF-Smt3 with HA-GBP-Cdc5 or HA-GBP-Cdc5^{KD} (4701-6-4, 4871-1-3, 4702-3-4, and 4913-4-4) were arrested with HU for 2 h at 30°C, and then cyanamide (8 mM) was added to induce either GBP-Cdc5 or GBP-*cdc5*^{KD} expression. Cells were collected every 30 min for western blotting to detect SUMO conjugates with anti-FLAG antibody. The level of GBP-Cdc5/Cdc5^{KD} was determined with anti-HA antibody. Pgk1, loading control. **(C)** Tof2 undergoes nucleolar delocalization upon Cdc5–Ulp2 tethering. Cells with the indicated genotypes (4700-3-2, 4862-8-1, and 4703-2-4) were arrested in HU for 2 h at 30°C before the addition of cyanamide. Cell samples before and after cyanamide treatment were taken to examine Tof2-mApple intensity. Scale bar, 5 µm. The average Tof2 intensity for each time point (n = 50 cells) was quantified. Statistical analysis used two-way ANOVA with Tukey's test. The bar graph represents mean values ± SD. **** $p < 0.0001$. **(D)** GBP-induced Cdc5–Ulp2 interaction triggers polySUMO-dependent Tof2 degradation. Cells with the indicated genotypes (4701-6-4, 4871-1-3, 4702-3-4, 4737-4-3, and 4913-4-4) were arrested with HU for 2 h at 30°C, and then cyanamide was added to induce GBP-Cdc5/Cdc5^{KD} expression. Western blotting was performed with anti-myc antibody to detect Tof2-13myc levels. Pgk1, loading control. Relative Tof2 protein levels (Tof2/Pgk1) for each strain were plotted on the graph. Source data are available for this figure: SourceData F3.

band shift was observed in the *ulp2*^{S734A} mutant (Fig. 4 C). Phosphatase treatment of IPed WT Ulp2 caused disappearance of this band shift (Fig. 4 D). Consistently, *in vitro* kinase assays confirmed that Ulp2^{S734A} was resistant to phosphorylation by Cdc5 kinase (Fig. 4 E). We also noticed that Ulp2^{S734A} retained partial phosphorylation both *in vivo* and *in vitro*. Using synchronized cells, we observed cell cycle–regulated band shift of Ulp2^{S734A}, although the band shift exhibited a 20-min delay compared with WT (Fig. S1), indicating that Ulp2 likely contains additional phosphorylation sites targeted by Cdc5 or other kinases. Together, these findings suggest that Ulp2^{S734} is likely the primary phosphorylation site regulated by Cdc5 kinase, although additional residues may also undergo phosphorylation.

If Ulp2^{S734} is a major phosphorylation site regulated by Cdc5, then *ulp2*^{S734A} mutant likely counteracts the effects triggered by Cdc5 overexpression. To test this idea, we examined the band shift of Ulp2 and Ulp2^{S734A} in HU-arrested cells overexpressing Cdc5 from the galactose promoter. As seen in Fig. 4 F, while Ulp2 exhibited a dramatic band-shift over time following Cdc5 overproduction, indicating increased phosphorylation, Ulp2^{S734A} exhibited minimal band shift under the same condition. In addition, Tof2 nucleolar delocalization and degradation induced by *CDC5* overexpression were also blocked in *ulp2*^{S734A} mutant cells (Fig. 4, G and H). Together, these results support the conclusion that Ulp2 S734 is an important phosphorylation site responsible for the regulation of polySUMOylation.

Phosphodeficient *ulp2*^{S734A} mutant shows delayed cell cycle progression

To understand the biological significance of Ulp2 phosphorylation at S734, we first assessed how *ulp2*^{S734A} mutation affects cell growth when Cdc5 is overexpressed. We found that the severe growth defect caused by *CDC5* overexpression was suppressed by the *ulp2*^{S734A} mutant (Fig. 5 A). We speculated that this suppression is likely due to the blockage of Cdc5-induced polySUMOylation. In that case, we expected chainless SUMO mutant

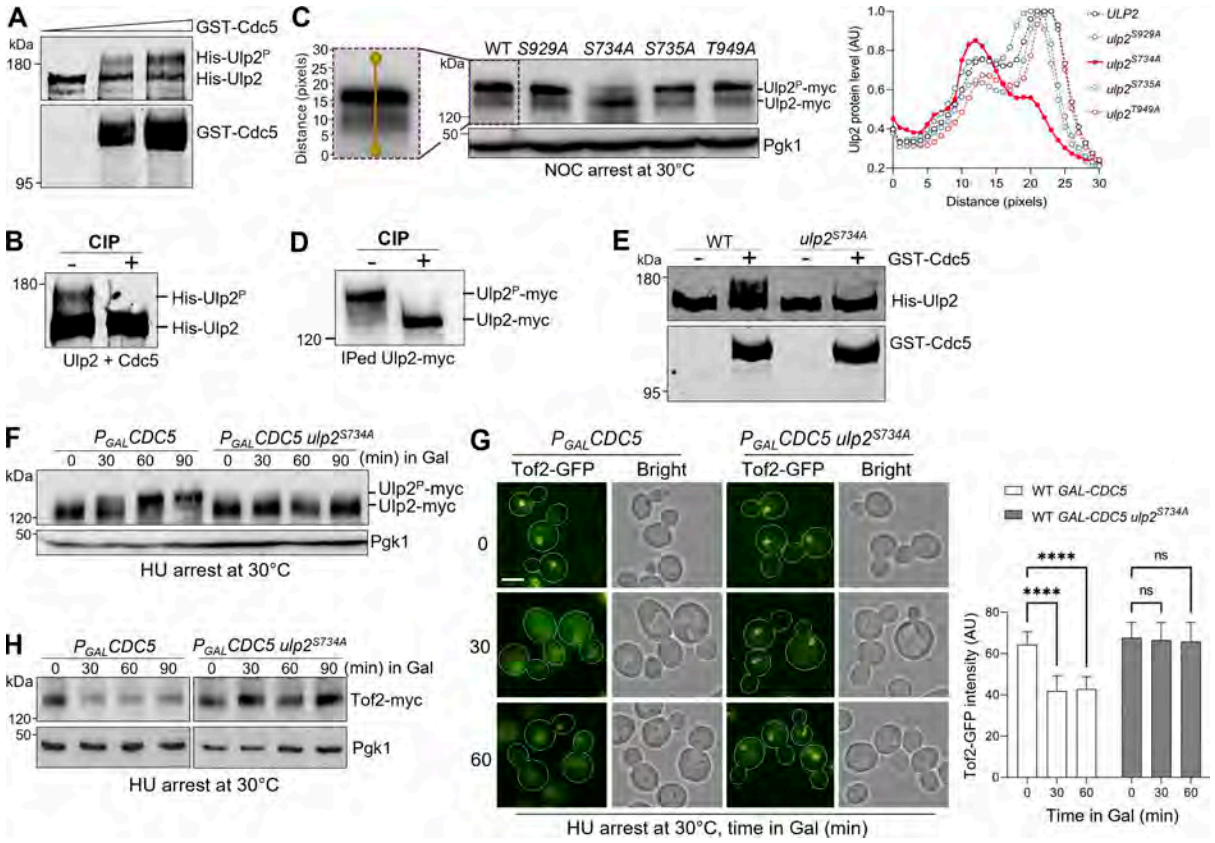

Figure 4. **Ulp2 S734 is the major phosphorylation site targeted by Cdc5 kinase. (A)** Ulp2 shows Cdc5 kinase–dependent phosphorylation *in vitro*. Ulp2 and Cdc5 were expressed from bacteria and purified. An *in vitro* kinase assay was performed by incubating both proteins together for 2 h at 30°C. Samples were collected for western blotting to detect Ulp2 and Cdc5 with anti-His and anti-GST antibodies, respectively. **(B)** Phosphatase treatment abolishes the slow migrating band of Ulp2 resulting from *in vitro* phosphorylation by Cdc5 kinase. Bacterially purified His-Ulp2 was incubated with GST-Cdc5 in a kinase buffer. The samples were treated with calf-intestinal phosphatase (CIP). Ulp2 was detected by western blotting with anti-His antibody. **(C)** The mutant Ulp2^{S734A} shows decreased phosphorylation *in vivo* compared with Ulp2. *ULP2-13myc* (YCH25), *ulp2^{S929A}-13myc* (EGM56), *ulp2^{S734A}-13myc* (EGM51), *ulp2^{S735A}-13myc* (EGM58), and *ulp2^{T949A}-13myc* (EGM52) cells were arrested in nocodazole for 2 h at 30°C before they were collected for western blotting (6% gel) with anti-myc antibody. Pgk1, loading control. Graph is representative of the Ulp2 phosphorylation level in WT and mutants (first peak represents hypo-phosphorylated Ulp2, second peak represents phosphorylated Ulp2). **(D)** The slow migrating band of Ulp2 from yeast cells disappeared after phosphatase treatment. Yeast extracts from nocodazole arrested *ULP2-13myc* (YCH25) cells were IPed with anti-myc antibody. After treatment with or without CIP, Ulp2 band shift was examined after western blotting with anti-myc antibody. **(E)** Ulp2^{S734A} shows less efficient phosphorylation than WT Ulp2 *in vitro*. Bacterially purified WT Ulp2 and Ulp2^{S734A} were subjected to Cdc5 kinase assay as described in A. Samples were collected for western blotting to detect Ulp2 and Cdc5. **(F)** The band shift of Ulp2 triggered by *CDC5* overexpression is impaired for Ulp2^{S734A}. HU-arrested *ULP2-13myc* (YCH26) and *ulp2^{S734A}-13myc* (EGM54) cells harboring the P_{GAL}*CDC5* plasmid in 30°C raffinose media were treated with galactose (2%) to induce Cdc5 overproduction. Cells were collected every 30 min for western blotting (6% gel) with anti-myc antibody. Pgk1, loading control. **(G)** Tof2 delocalization upon Cdc5 overproduction is blocked in *ulp2^{S734A}* mutants. HU-arrested WT (EGM43) and *ulp2^{S734A}* (4971-2-1) cells containing Tof2-GFP and the P_{GAL}*CDC5* plasmid in 30°C raffinose media were treated with galactose (2%). Scale bar, 5 µm. Samples were taken at the indicated time points, and the average Tof2-GFP intensity (n = 50 cells) was quantified. Statistical analysis used two-way ANOVA with Tukey's test. The bar graph represents mean values ± SD. **** $p < 0.0001$. **(H)** Cdc5-triggered Tof2 degradation is dependent on Ulp2 phosphorylation at S734. WT (YYW273) and *ulp2^{S734A}* (4962-1-2) cells with Tof2-13myc and P_{GAL}*CDC5* were arrested with HU in 30°C raffinose medium. Then galactose was added to induce *CDC5* overexpression. Western blotting was performed with anti-myc antibody. Pgk1, loading control. Source data are available for this figure: SourceData F4. IPed, immunoprecipitated.

smt3-KRall to show similar suppression. Indeed, *smt3-KRall* mutants also exhibited much better growth than control cells when *CDC5* was overexpressed. If the phosphorylation of Ulp2 S734 regulates polySUMOylation, we expected some cell cycle defects for *ulp2^{S734A}* mutant cells. In comparison with WT, *ulp2^{S734A}* cells exhibited slightly slower growth on plates at different temperatures as well as delayed disappearance of large-budded cells after G_1 release (Fig. 5, B and C), indicating a possible cell cycle delay. Protein sequence analysis reveals that this phosphorylation site is not conserved in other *Saccharomyces* species, such as *Saccharomyces kudriavzevii* (Fig. 5 D). Thus, it is unclear whether other organisms share the same mechanism to regulate polySUMOylation via Ulp2 phosphorylation.

Because polySUMOylation promotes Tof2 nucleolar delocalization (Gutierrez-Morton et al., 2024), we monitored Tof2-GFP fluorescence intensity throughout the cell cycle in WT and *ulp2^{S734A}* cells after G_1 release. The Tof2-GFP intensity in WT cells showed an increase after G_1 release, peaking at 60 min, followed by a sharp decline at 80 min (Fig. 6 A). In contrast, *ulp2^{S734A}* mutants exhibited relatively persistent nucleolar Tof2-GFP

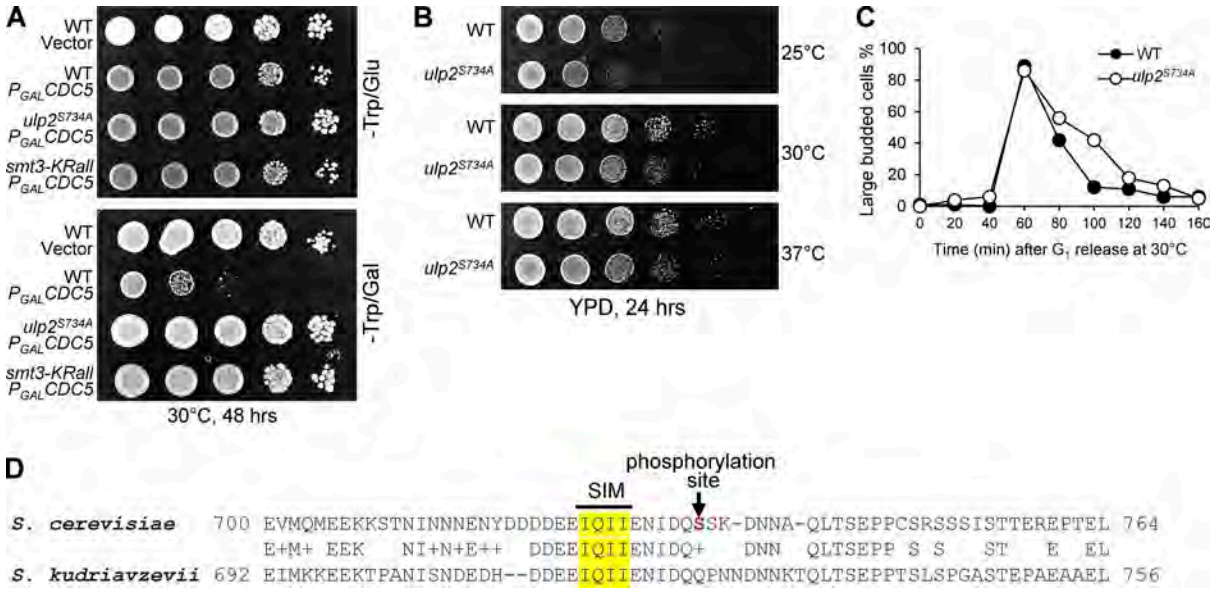

Figure 5. **The growth phenotype of phosphodeficient *ulp2*^{S734A} mutants. (A)** *ulp2*^{S734A} and SUMO chainless *smt3-KRall* mutants restore the viability of cells with overexpressed Cdc5. *ULP2-13myc* (YCH26), *ulp2*^{S734A}*-13myc* (EGM54), and *smt3-KRall* (HY8053) cells containing the P_{GAL}*CDC5* plasmid were grown to saturation, then 10-fold serially diluted and spotted onto -TRP + 2% glucose/galactose dropout plates. The plates were incubated for 48 h at 30°C before imaging. WT (Y300) cells containing the vector (pBAD104) or P_{GAL}*CDC5* plasmid were used as controls. **(B)** *ulp2*^{S734} mutants show minor sick growth on plates. *ULP2-13myc* (YCH25) and *ulp2*^{S734A}*-13myc* (EGM51) cells were grown to saturation, then 10-fold serially diluted and spotted onto YPD plates. Plates were incubated at 25°C, 30°C, and 37° for 24 h before imaging. **(C)** *ulp2*^{S734A} cells show a slight delay in cell cycle progression. G_1-arrested *ULP2-13myc* (YCH25) and *ulp2*^{S734A}*-13myc* (EGM51) cells were released into the cell cycle. Cells were collected every 20 min for budding index. **(D)** Protein sequence alignment of the regions surrounding the SIM of Ulp2 from *S. cerevisiae* and *S. kudriavzevii*. The SIM and phosphorylation site in Ulp2 are marked.

signal after peaking at 60 min. Additionally, *ulp2*^{S734A} mutants showed a 20-min delay in nucleolar separation (Fig. 6 A). We also compared the kinetics of Tof2 degradation during the cell cycle in WT and *ulp2*^{S734A} cells using western blotting. Tof2 degradation was significantly impaired in *ulp2*^{S734A} cells compared with WT in the late points (Fig. 6 B). The delayed Tof2 delocalization and degradation in phosphodeficient *ulp2*^{S734A} cells suggests the positive role of Ulp2 S734 phosphorylation in polySUMOylation. Moreover, comparison of bulk SUMOylation of metaphase cells arrested with nocodazole showed an appreciable accumulation of SUMOylated conjugates in WT cells (Fig. S2). However, less SUMO conjugates were detected in either *cdc5-2* or phosphodeficient *ulp2*^{S734A} cells. We speculate that more active Ulp2 in these mutants decreases the level of polySUMOylation, reducing the intensity of SUMO conjugates.

We previously showed that Tof2 nucleolar delocalization and degradation occurred in *cdc15-2*–arrested telophase cells (Gutierrez-Morton et al., 2024). Therefore, we followed Tof2 localization in *cdc15-2*–arrested telophase cells with *ULP2* or *ulp2*^{S734A}. We observed a notable decrease in Tof2-GFP signal intensity and protein levels in *cdc15-2* single mutant following cell cycle arrest at 37°C for 2 h, indicating Tof2 degradation (Fig. 6 C). In contrast, *cdc15-2 ulp2*^{S734A} cells retained a persistent Tof2-GFP signal and Tof2 protein level, suggesting that Tof2 delocalization and degradation are impaired in *ulp2*^{S734A} mutant. These data highlight the critical role of Ulp2 S734 phosphorylation in facilitating Tof2 delocalization and turnover during the cell cycle.

Tof2 is a nucleolar anchor of Cdc14, and its nucleolar delocalization and degradation cause partial Cdc14 release for mitotic exit (Gutierrez-Morton et al., 2024; Waples et al., 2009). Fin1 dephosphorylation by Cdc14 enables its kinetochore binding (Bokros et al., 2016; Bremmer et al., 2012). Thus, we used kinetochore localization of Fin1 as a readout for Cdc14 activation. After 2-h incubation of *cdc15-2* cells at 37°C, the majority (97%) showed kinetochore-localized Fin1 (Fig. 6 D), indicating robust Cdc14 activation. In polySUMO-deficient *cdc15-2 smt3-KRall* cells, the frequency of Fin1 localization at the kinetochore decreased to 75%. Interestingly, *cdc15-2 ulp2*^{S734A} cells displayed 88% Fin1-kinetochore localization: higher than *cdc15-2 smt3-KRall* cells but significantly lower than *cdc15-2* cells alone. Therefore, phosphodeficient *ulp2*^{S734A} mutants exhibit compromised Cdc14 activation. Together, these results suggest that Ulp2 phosphorylation at S734 promotes polySUMOylation and downstream processes, including Cdc14 activation, at least in partial.

PP2A^{Rts1} promotes Ulp2 S734 dephosphorylation

A protein phosphatase likely counteracts Cdc5-dependent Ulp2 phosphorylation. To investigate the mechanism underlying Ulp2 dephosphorylation, we focused on PP2A, given its multiple roles in mitotic regulation. The PP2A holoenzyme is comprised of three subunits: a scaffolding subunit (Tpd3), a regulatory subunit (Cdc55 or Rts1), and a catalytic subunit (Pph21, Pph22, or Pph3) (Sneddon et al., 1990). Both Cdc55 and Rts1 are implicated in mitotic processes, with Cdc55 coordinating Cdc14 release and Rts1 modulating sister chromatid separation and the spindle assembly checkpoint (Jin et al., 2017; Queralt et al., 2006; Wang and Ng, 2006; Yellman and Burke, 2006). Because PP2A regulatory subunits confer substrate specificity, we determined if

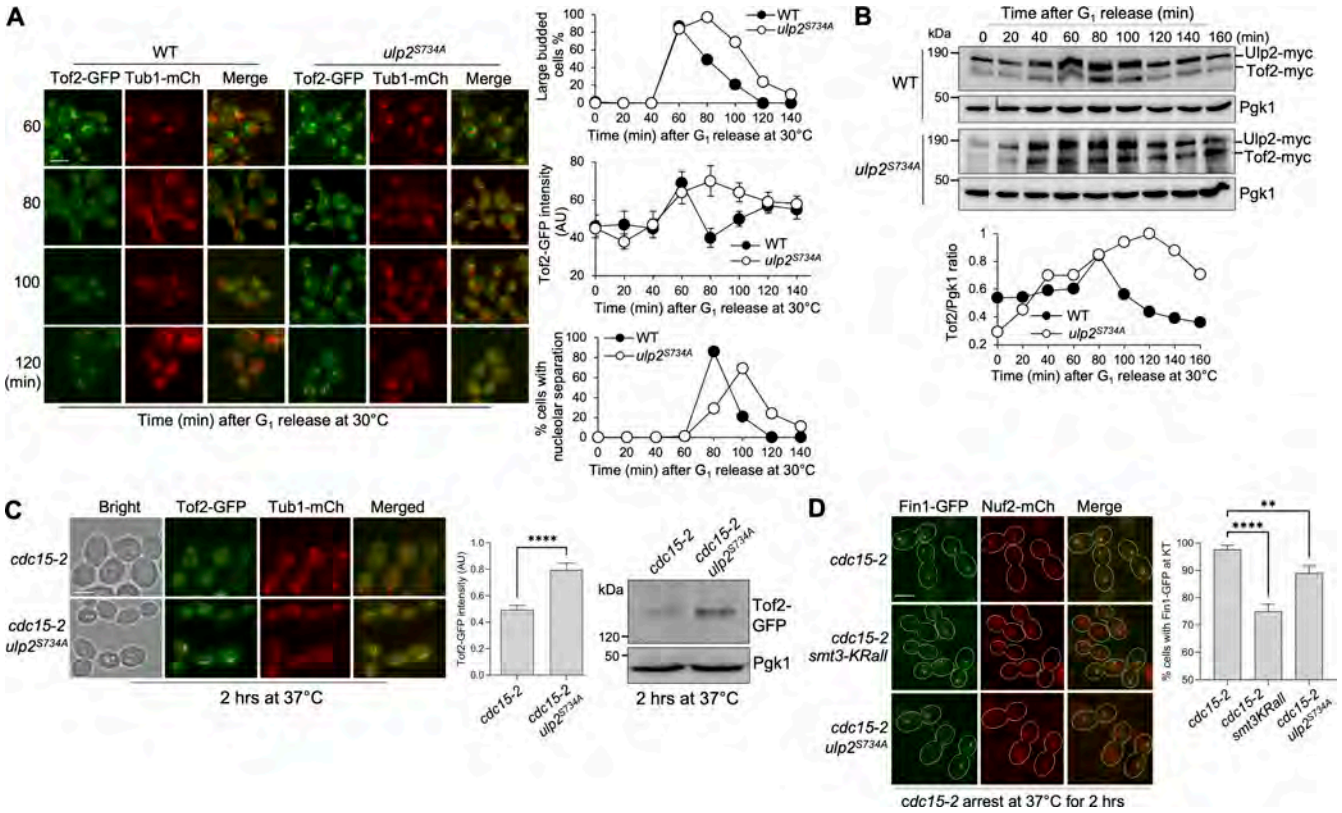

Figure 6. **The phosphodeficient *ulp2^{S734A}* mutant shows cell cycle defects. (A)** *ulp2^{S734A}* mutant cells exhibit persistent Tof2-GFP intensity and delayed nucleolar separation. G_1-arrested WT (4822-11-1) and *ulp2^{S734A}* (4900-4-3) mutant cells expressing Tof2-GFP were released into the cell cycle at 30°C, and cells were taken over time for budding index (top graph) and the examination of Tof2-GFP intensity. Scale bar, 5 µm. Tub1-mCherry, spindle marker. The average Tof2-GFP intensity for each time point (n = 50 cells) was quantified, and the line graph represents mean values ± SD (center graph). The percentage of cells with nucleolar separation during the cell cycle is plotted (bottom graph). **(B)** PolySUMO-dependent Tof2 degradation during the cell cycle is compromised in *ulp2^{S734A}* mutant cells. G_1-arrested WT (4973-1-1) and *ulp2^{S734A}* (4962-1-2) cells with Tof2-13myc were released into the cell cycle at 30°C. Cells were collected every 20 min for western blotting with anti-myc antibody and budding index. In these strains, both Ulp2 and Tof2 are tagged with myc. Pgk1, loading control. The graph shows the relative Tof2 protein level (Tof2/Pgk1 ratio) over time. **(C)** Tof2 nucleolar delocalization is compromised in *ulp2^{S734A}* mutant cells. Asynchronous *cdc15-2* (4822-8-2) and *cdc15-2 ulp2^{S734A}* (4900-3-3) cells with Tof2-GFP and Tub1-mCherry were shifted to 37°C for 2 h to inactivate Cdc15 for telophase arrest. Samples were taken to examine Tof2-GFP signal and spindle morphology (Tub1-mCherry). The average Tof2-GFP intensity (n = 50 cells) was quantified. Statistical analysis used unpaired t test, and the graph represents mean values ± SD. **** $p < 0.0001$. Scale bar, 5 µm. Samples were also taken to examine Tof2-GFP protein level with anti-GFP antibody (right). Pgk1, loading control. **(D)** Phosphodeficient *ulp2^{S734A}* mutation delays Fin1-GFP kinetochore localization during the cell cycle. Asynchronous *cdc15-2* cells (4635-2-3) with *smt3-KRall* (4635-3-3) or *ulp2^{S734A}* (4970-3-2) harboring *FIN1-GFP* plasmid (pSB1252) were shifted to 37°C for 2 h for telophase arrest. Fin1-GFP kinetochore localization in representative cells is shown. Nuf2-mCherry, a kinetochore marker. Scale bar, 5 µm. Fin1 kinetochore localization was quantified after three repeats. Statistical analysis used one-way ANOVA with Tukey's test. Bars represent mean values ± SD. ** $p < 0.01$, **** $p < 0.0001$. Source data are available for this figure: SourceData F6.

Cdc55 and Rts1 play a role in Ulp2 phosphorylation by arresting cells in mitosis, where a portion of Ulp2 is phosphorylated in WT cells (Fig. 7 A). In these cells, trace protein polySUMOylation was also detected. We observed that the loss of Rts1 or Pph21/Pph22 led to enhanced Ulp2 phosphorylation. Additionally, increased polySUMOylation was detected in these mutants, similar to the increase in *ulp2Δ* cells. Interestingly, deletion of *CDC55* did not cause a significant change in Ulp2 phosphorylation but did show a decrease in SUMOylation for an unknown reason. These findings suggest that PP2A^{Rts1} facilitates Ulp2 dephosphorylation, potentially preventing untimely polySUMOylation.

To determine if Rts1 counteracts Cdc5-dependent phosphorylation of Ulp2 S734, we compared Ulp2 phosphorylation in *rts1Δ* and *rts1Δ ulp2^{S734A}* cells. Strikingly, the Ulp2 hyperphosphorylation observed in *rts1Δ* cells diminished in *rts1Δ ulp2^{S734A}* mutants (Fig. 7 B), indicating PP2A^{Rts1} is required for Ulp2 S734 dephosphorylation. We further examined Ulp2 phosphorylation dynamics during the cell cycle in *rts1Δ* mutants and found that loss of Rts1 caused delayed Ulp2 dephosphorylation in comparison with WT cells (Fig. S3). Moreover, a portion of sustained Ulp2 band shift was visible across the cell cycle in *rts1Δ* cells, indicating upregulated Ulp2 phosphorylation. We next investigated whether the loss of Rts1 could lead to premature delocalization and degradation of SUMO substrate Tof2 as a result of polySUMOylation. In Fig. 7, C and D, we analyzed Tof2-GFP fluorescence intensity and Tof2-myc protein level in *cdc13-1* mutant cells, which arrest at pre-anaphase at high temperatures due to DNA damage checkpoint activation (Liang and Wang, 2007). After a 2-h incubation at 37°C, most *cdc13-1* cells showed stabilized Tof2-GFP fluorescence signal and protein level. However, Tof2 fluorescence signal intensity as well as protein level decreased considerably in the *cdc13-1 rts1Δ* mutants,

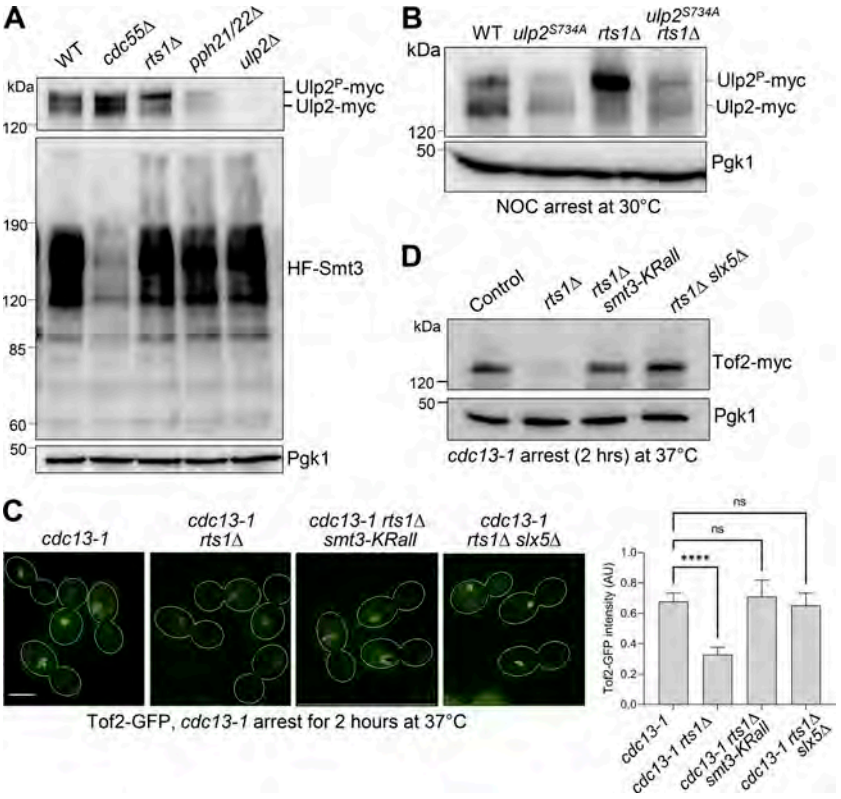

Figure 7. **Ulp2 dephosphorylation depends on PP2A^{Rts1} phosphatase. (A)** *RTS1* deletion leads to Ulp2 hyperphosphorylation and triggers polySUMOylation in nocodazole-arrested yeast cells. Asynchronous *ULP2-13myc* or *HF-SMT3* cells with the indicated PP2A mutant genotypes (4898-3-3, 4804-1-2, 4805-1-1, 4786-5-3, 4801-2-2, 4806-7-2, 4807-4-2, and 4675-2-2) were treated with nocodazole for 2 h at 30°C to achieve mitotic arrest. Samples were collected for western blotting with anti-FLAG to detect the levels of SUMOylation (HF-Smt3) and anti-myc antibodies to examine Ulp2 phosphorylation (6% gel for anti-myc western blotting). Pgk1, loading control. **(B)** Ulp2 hyperphosphorylation in *RTS1* deletion mutants is suppressed by the *ulp2^{S734A}* mutation. WT (YCH25) and mutants with the indicated genotypes (EGM51, 4786-5-3, and 4904-2-1) were treated the same as in A to detect the band shift of Ulp2-13myc. Pgk1, loading control. **(C)** Premature Tof2 nucleolar delocalization in the absence of Rts1 is polySUMO dependent. *cdc13-1* cells with the indicated genotypes (4347-10-1, 4525-1-1, and 4940-1-3) were shifted to 37°C for 2 h for pre-anaphase arrest. Cell samples were collected to examine Tof2-GFP intensity. Scale bar, 5 µm. The average Tof2-GFP intensity (n = 50 cells) was quantified, and statistical analysis used one-way ANOVA with Tukey's test. The bar graph represents mean values ± SD. **** $p < 0.0001$. **(D)** Untimely Tof2 turnover in *rts1Δ* mutants is suppressed in polySUMO axis mutants. *cdc13-1* (4949-1-1), *cdc13-1 rts1Δ* (4949-2-2), and *cdc13-1 rts1Δ* mutants in combination with *smt3-KRall* or *slx5Δ* (4950-1-4 and 4966-2-3) were shifted to 37°C for 2 h to achieve pre-anaphase arrest. Then, cell samples were collected for western blotting to detect Tof2-13myc protein level with anti-myc antibody. Pgk1, loading control. Source data are available for this figure: SourceData F7.

indicative of protein delocalization and turnover. Notably, this decrease in Tof2 level was rescued by *smt3-KRall* or *slx5Δ*, suggesting that the decrease depends on the polySUMO axis. Overall, we conclude that PP2A^{Rts1} counteracts Ulp2 phosphorylation, which retains Ulp2 activity to prevent premature polySUMOylation during the cell cycle.

Ulp2 phosphorylation weakens SUMO chain binding

As a SUMO protease, Ulp2 binds to SUMO chains and cleaves SUMOs at their distal ends (Eckhoff and Dohmen, 2015). Ulp2 contains a SIM between residues 725 and 728 that is required for its SUMO chain binding and proteolytic activity, both *in vivo* and *in vitro* (de Albuquerque et al., 2018). Interestingly, as depicted in Fig. 8 A, the Ulp2 SIM is close to the S734 phosphorylation site. Thus, one possibility is that Ulp2 phosphorylation at S734 introduces negative charges, thereby impairing the electrostatic interactions between its SIM domain and polySUMOylated substrates. To test this idea, we first used fluorescence anisotropy to measure the interaction between a purified, fluorescently labeled 4×Smt3 protein and several forms of a recombinant, catalytically inactive Ulp2 fragment (residues 407–767, C624A) consisting of the full catalytic domain as well as the C-terminal region surrounding S734 and the SIM (Fig. S4, A and B). We found this region sufficient to bind 4×Smt3 in an apparent 1:1 stoichiometry by gel filtration (Fig. 8 B).

Titration of increasing concentrations of the WT Ulp2 fragment against a constant concentration of the fluorescent 4×Smt3 yielded a hyperbolic curve that fit well to a 1:1 binding model with a dissociation constant (K_D) of 1.0 ± 0.2 µM (Fig. 8 C). This value is significantly lower than the reported affinity of the Ulp2 SIM alone for 4×Smt3 (de Albuquerque et al., 2018), as would be expected for cooperative binding between the SIM and the catalytic domain. Importantly, when phosphoserine was genetically incorporated at position 734 using a published approach (Zhu et al., 2019), the affinity for 4×Smt3 was weakened ~3.4-fold (Fig. 8 D), supporting the idea that Ulp2 phosphorylation at S734 introduces negative charges and weakens the electrostatic interactions between its SIM domain and polySUMOylated substrates. Similarly, a phospho-mimetic mutant Ulp2 fragment, S734E, displayed an approximately twofold weaker affinity for 4×Smt3 compared with the unphosphorylated WT Ulp2 fragment (Fig. 8 E). As expected, no binding to 4×Smt3 was observed for an unrelated protein, yeast Rpn10 (Fig. 8 F), supporting the specificity of our binding assay for the Ulp2–4×Smt3 interaction. Together, these data indicate that the nature of the amino acid side chain at position 734 in Ulp2 influences its affinity for Smt3 and show that introduction of negative charges, either by phosphorylation or via mutation, weakens the affinity of Ulp2 for 4×Smt3.

We next examined the interaction between Ulp2 and SUMOylated proteins in both WT and phosphodeficient *ulp2^{S734A}*

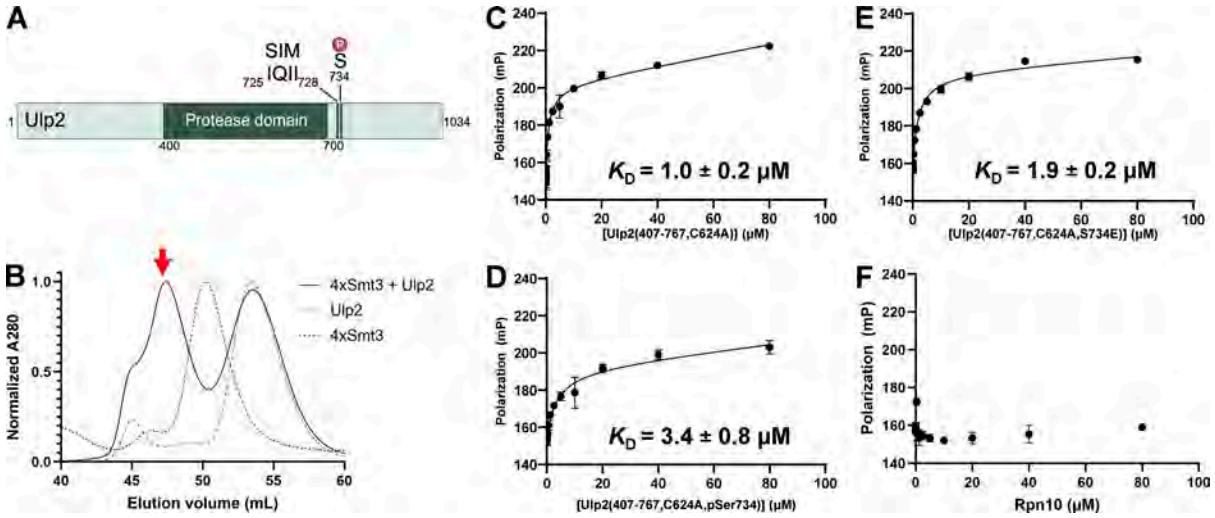

Figure 8. **Ulp2 phosphorylation at S734 weakens its SUMO chain binding ability *in vitro*. (A)** The Ulp2 SIM domain (residues 725–728) is near phosphorylation site, S734. **(B–F)** Validation of interaction between Ulp2 (407–767, C624A)-6xHis and unlabeled 4×Smt3 by gel filtration. The leftward shift of the elution peak (red arrow) upon mixing the two proteins indicates their interaction. The interaction between 250 nM Oregon Green 488–labeled 4×Smt3 and an unphosphorylated (C), S734-phosphorylated (D), or S734E mutant (E) Ulp2 fragment was measured by fluorescence polarization. Affinities shown represent the mean ± SD of three independent measurements. The proteasome subunit Rpn10, a protein not known to bind Smt3, was included as a negative control (F).

mutant cells. After IP of HF-Smt3 using the anti-FLAG antibody from cell lysates, our results revealed that Ulp2 interacts with SUMOylated proteins in asynchronous WT cells (Fig. 9 A, lane 4). However, the phosphodeficient Ulp2^{S734A} exhibited a stronger interaction based on the amount of Ulp2 proteins pulled down by HF-Smt3 (lane 5). Similarly, more Ulp2 was detected in nocodazole-arrested *ulp2^{S734A}* cells after HF-Smt3 IP compared with WT cells (lanes 6 and 7). These data, coupled with our affinity measurements, support our hypothesis that Ulp2 phosphorylation at S734 interferes with its interaction with SUMOylated proteins.

Furthermore, we examined whether Cdc5 overproduction, which triggers Ulp2 phosphorylation, affects the interaction between Ulp2 and SUMO chains. To this end, we arrested WT and *ulp2^{S734A}* cells in HU to prevent endogenous Cdc5 expression and then induced Cdc5 overexpression by adding galactose. After HF-Smt3 IP with anti-FLAG antibody, we observed that Cdc5 overproduction significantly weakened the interaction between Ulp2 and SUMOylated proteins (lanes 4 and 6 in Fig. 9 B). Notably, this interaction was restored in the phosphodeficient *ulp2^{S734A}* mutant (lanes 5 and 7 in Fig. 9 B). In a similar experiment, we compared the interaction between Ulp2 and SUMOylated proteins in WT, *rts1Δ*, and *rts1Δ ulp2^{S734A}* cells. Because Ulp2 hyperphosphorylation in *rts1Δ* mutant results in polySUMO-mediated protein turnover, we used proteasome inhibitor MG-132 to prevent this turnover. Shown in Fig. 9 C, we observed impaired binding of Ulp2 to SUMOylated substrates in *rts1Δ* mutant (lane 5), but this decrease was suppressed by *ulp2^{S734A}* mutation, at least partially (lane 6). Taken together, these *in vitro* and *in vivo* findings indicate that phosphorylation at Ulp2 S734 impairs the interaction between Ulp2 and SUMOylated proteins, likely by altering the non-covalent protein–protein interactions at the interface between Ulp2's SIM and SUMO chains.

Discussion

In this study, we investigated the mechanisms by which Cdc5 kinase and PP2A^{Rts1} phosphatase control the timing of polySUMOylation during the cell cycle in budding yeast by targeting Ulp2, the SUMO protease that cleaves SUMO chains and prevents polySUMOylation. Our findings demonstrate that Cdc5 kinase promotes polySUMOylation and polySUMO-mediated cell cycle processes. Using a chemical-genetic approach, we found that tethering Cdc5 to Ulp2 is sufficient to induce polySUMOylation and its downstream processes. Moreover, we demonstrated that both Cdc5 kinase and PP2A^{Rts1} phosphatase regulate Ulp2 phosphorylation. We also discovered that Ulp2 phosphorylation at S734 reduces its affinity for SUMO chains. Together, these findings present a detailed framework for understanding how Cdc5 kinase and PP2A^{Rts1} phosphatase-regulated Ulp2 phosphorylation controls polySUMOylation dynamics during the cell cycle (Fig. 9 D).

Our findings suggest that Ulp2 phosphorylation at S734 induces polySUMOylation. Phosphodeficient *ulp2^{S734A}* mutants exhibit decreased SUMO conjugates similar to *cdc5-2* mutants. Additionally, *ulp2^{S734A}* mutants showed delayed Tof2 delocalization and turnover, which depends on polySUMOylation. Functional studies of the *ulp2^{S734A}* mutant revealed impaired kinetochore localization of Fin1, a Cdc14-dependent process; however, this phenotype was less severe than that observed in the chainless SUMO mutant *smt3-KRall*. This indicates that phosphorylation at Ulp2 S734, while significant, is not the sole determinant of Ulp2's regulation. Additional phosphorylation sites on Ulp2 likely weaken its enzyme activity as well, thereby promoting polySUMOylation and mitotic exit. In line with this, several studies revealed that Ulp2 is also phosphorylated by the cyclin-dependent kinase in budding yeast (Baldwin et al., 2009; Holt et al., 2009; Ubersax et al., 2003). Moreover, it remains unclear whether S734 is the only site targeted by Cdc5 kinase.

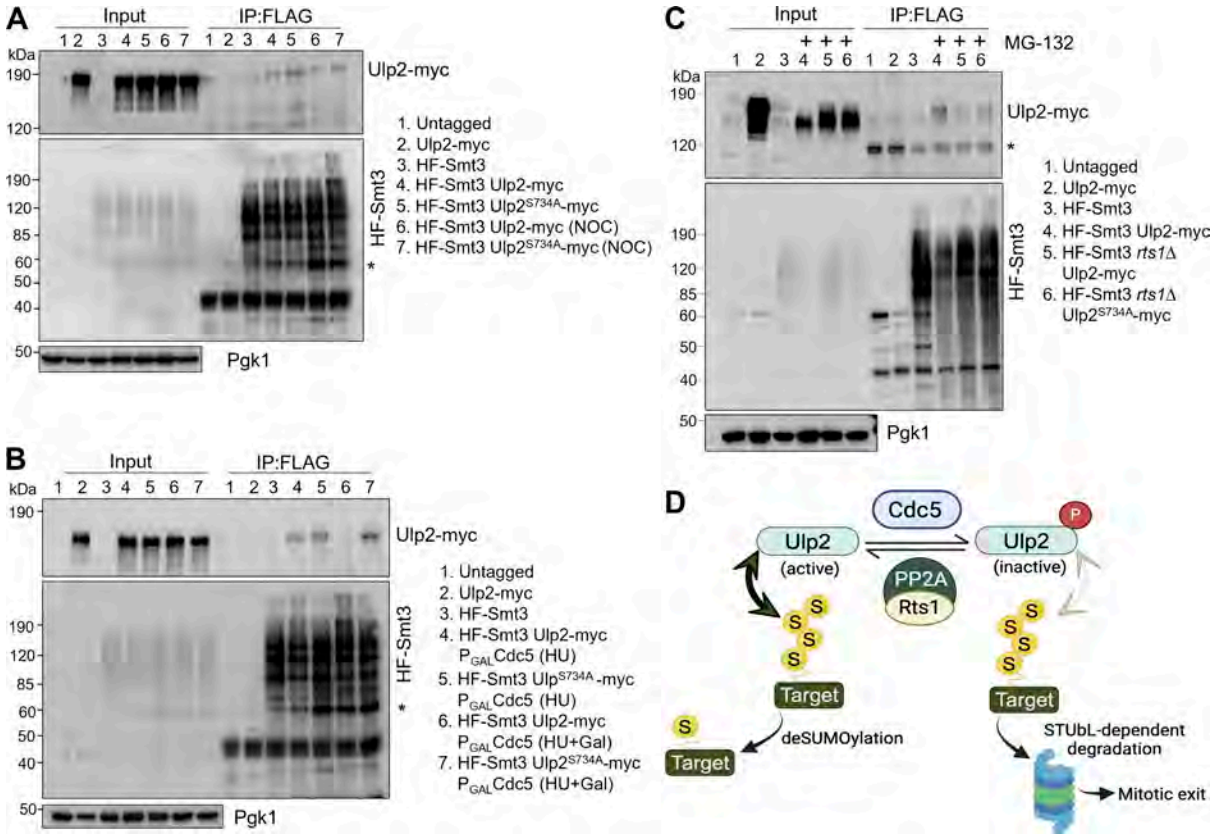

Figure 9. **Ulp2 phosphorylation at S734 reduces its binding to SUMOylated protein species *in vivo*. (A)** SUMO substrate binding of Ulp2 is enhanced in phosphodeficient mutants *ulp2*^{S734A}. *HF-SMT3* cells with the indicated genotypes (4898-3-3 and 4903-3-1) growing asynchronously or in a nocodazole arrest for 2 h at 30°C were collected for IP with anti-FLAG antibody. After precipitating HF-Smt3 conjugates, HF-Smt3 and Ulp2/Ulp2^{S734A}-13myc protein levels in the input and IPed fraction were detected by western blotting with anti-FLAG and anti-myc antibodies. WT (Y300, untagged), *HF-SMT3*, and *ULP2-13myc* strains served as negative controls. Pgk1, loading control. * denotes nonspecific binding. **(B)** *CDC5* overexpression disrupts the binding of Ulp2 to SUMO substrates, while the *ulp2*^{S734A} mutant restores this binding. *ULP2-13myc* and *ulp2*^{S734A}*-13myc* cells (4898-3-3 and 4903-3-1) harboring plasmid P_{GAL}*CDC5* were arrested in HU for 2 h in 30°C raffinose media. Then, 2% galactose was added to induce Cdc5 overproduction for 2 h. Cell extracts were collected and IPed with anti-FLAG antibody to isolate HF-Smt3 conjugates. HF-Smt3 and Ulp2-13myc protein levels in the input and IPed fraction were detected by western blotting. WT (Y300, untagged), *HF-SMT3*, and *ULP2-13myc* cells served as negative controls. Pgk1, loading control. * denotes nonspecific binding. **(C)** Reduced binding of Ulp2 to SUMO substrate in *rts1Δ* mutant cells is restored in *rts1Δ ulp2*^{S734A} double mutants. Cells (4898-3-3, 4942-1-2, and 4967-2-3) growing asynchronously at 30°C were treated with a proteasome inhibitor MG-132 for 1 h before cell extracts were collected for IP. After isolating HF-Smt3 conjugates with anti-FLAG antibody, HF-Smt3 and Ulp2-13myc protein levels in the input and IPed fraction were detected by western blotting with anti-FLAG and anti-myc antibodies, respectively. WT (Y300, untagged), *HF-SMT3*, and *ULP2-13myc* cells served as negative controls. Pgk1, loading control. * denotes nonspecific binding. **(D)** The working model for the regulation of polySUMOylation during cell cycle. Cdc5 kinase–dependent phosphorylation of SUMO protease Ulp2 weakens its SUMO chain binding, triggering polySUMOylation, while PP2A^{Rts1} phosphatase counteracts this modification to prevent premature polySUMOylation. Source data are available for this figure: SourceData F9. IPed, immunoprecipitated.

Surprisingly, this phosphorylation site is not conserved in other *Saccharomyces* species, such as *S. kudriavzevii* (Fig. 5 D). While S734 is not conserved among Ulp2 orthologs, the regulation of SUMO–SIM interaction by phosphorylation may be a conserved principle. Thus, the specific residue might vary across different species. Although our findings indicate that Ulp2 S734 is the primary phosphorylation site to regulate its activity, we acknowledge that further evidence is needed to verify this. In addition, we cannot exclude the possibility that multiple phosphorylation sites ensure robust control over Ulp2 activity.

Cdc5 overexpression is lethal (Fig. 5 A) (Mishra et al., 2019). Interestingly, we found that phosphodeficient *ulp2*^{S734A} and SUMO chainless *smt3-KRall* mutants suppressed the lethality caused by Cdc5 overproduction. This finding suggests that Ulp2 phosphorylation and inactivation likely play a major role in the lethality caused by Cdc5 overexpression. Then, an interesting question is why *ulp2Δ* mutant is not lethal. One explanation is that although *ulp2Δ* cells exhibit severe growth defects, they rapidly accumulate survivors with aneuploidy (Li and Hochstrasser, 2000; Ryu et al., 2016). The tendency of the *ulp2Δ* mutant to form aneuploid survivors may facilitate the expression of suppressors for the growth defect of *ulp2Δ* cells. Another consideration is that the lethality caused by Cdc5 overexpression could be a combination of Ulp2 inactivation and disruption of other cellular functions given the numerous substrates targeted by Cdc5 kinase, but phosphodeficient *ulp2*^{S734A} is sufficient to suppress this lethality. Under these conditions, Ulp2 may play a key role in preventing the toxic buildup of polySUMOylated substrates and maintaining SUMO homeostasis.

Our evidence indicates that phosphorylation of Ulp2 at S734 weakens its binding to SUMO chains (Figs. 8 and 9). One possibility is that phosphorylated Ulp2 fails to bind SUMO chains through electrostatic interference. Ulp2 interacts with SUMO chains via its C-terminal SIM (residues 725–728), which relies on hydrophobic interactions between Ulp2 and SUMO (Song et al., 2004). Introducing a negative charge at residue 734 likely interferes with these interactions, thereby reducing Ulp2's ability to engage with SUMOylated substrates. Indeed, our *in vitro* results show that Ulp2 phosphorylation at S734 or the phosphomimetic mutation S734E reduces its binding to SUMO chains. Phosphorylation often targets flexible regions or intrinsically disordered protein domains. Over 60% of the C-terminal domain of Ulp2 is intrinsically disordered (Kroetz et al., 2009; Linding et al., 2003). The same is true for human Ulp2 orthologues SENP6 and SENP7 (Li et al., 2022; Lima and Reverter, 2008). These disordered regions are frequently associated with low-affinity, high-specificity protein–protein interactions (Dyson and Wright, 2005). The disordered regions in Ulp2 and its orthologues likely interact with SUMO chains by providing flexible binding interfaces, but Cdc5-dependent Ulp2 phosphorylation likely impairs this interaction. Another possibility is that Ulp2 phosphorylation may induce conformational changes in these disordered domains to reduce SUMO chain binding.

We provide evidence demonstrating Cdc5-dependent Ulp2 phosphorylation, but the mechanisms regulating Cdc5 during this process remain unclear. We propose the involvement of intermediary proteins. One plausible candidate is SUMO substrate Dbf4, as it is a known binding partner to both Cdc5 and Ulp2 (Hardy and Pautz, 1996; Kitada et al., 1993; Psakhye et al., 2019). As part of the Cdc7–Dbf4 complex (DDK), Dbf4 acts as a regulatory subunit required for initiating DNA replication. Additionally, Dbf4 binds to Cdc5 and facilitates Cdc7-mediated Cdc5 phosphorylation, which may prevent Cdc5 from recognizing its substrates involved in mitotic exit (Chen and Weinreich, 2010; Miller et al., 2009). Other evidence indicates that DDK can enhance Cdc5 kinase activity. For instance, Cdc5 binds to DDK, and together, they both phosphorylate and activate Mus81-Mms4 nuclease, allowing resolution of recombination structures (Princz et al., 2017). However, the precise mechanism by which Dbf4 recruits Cdc5 to Ulp2 has not been investigated. Other Cdc5 interactors that may also play a role in its recruitment to Ulp2 include cohesin subunit Scc1 (Alexandru et al., 2001) and histone H3 variant Cse4 (Mishra et al., 2019). Both Scc1 and Cse4, like Dbf4, are SUMO targets (Ohkuni et al., 2016; Wu et al., 2012). Interestingly, the interaction between Ulp2 and Dbf4 depends on Dbf4 SUMOylation (Psakhye et al., 2019), which raises the possibility that SUMOylation of these targets recruits Ulp2 to Cdc5. However, further investigation is required to clarify how these interactions regulate Ulp2 activity.

In addition to its phosphorylation, Ulp2 may also be regulated through other mechanisms, including spatiotemporal control. Ulp2 is known to localize the inner kinetochore complex CCAN through a kinetochore-interacting motif (Quan et al., 2021; Suhandynata et al., 2019). Furthermore, Ulp2 localizes to the nucleolus partially by interacting with the cohibin complex Csm1–Lrs4 (Liang et al., 2017). While Ulp2 activity may be constrained by its subcellular localization, the specific context of this regulation as well as whether it is cell cycle–dependent remain unclear. Additionally, Ulp2 protein levels show modest cell cycle–dependent fluctuation, implying that its turnover may also play a role in regulating its activity. Further studies are needed to clarify how subcellular localization and protein turnover, in addition to phosphorylation, could contribute to the regulation of Ulp2 activity and global SUMO homeostasis during the cell cycle. Another SUMO protease, Ulp1, localizes at nuclear pore complexes (de Albuquerque et al., 2016; Panse et al., 2003). One untested possibility is Ulp1 localization may be cell–cell regulated, which plays a role in controlling the timing of protein polySUMOylation.

Materials and methods

Yeast strains, growth, and media

The relevant genotypes and sources of the yeast strains used in this study are listed in Table S2. Several yeast strains used in this study were generated in our previous work, including Y300 (Wang et al., 2003), EMG2, 4802-4-1, YYW273, 4160-1-2, 4161-3-2, 4289-3-2, YCH25, 4635-2-3, and 4635-3-3 (Gutierrez-Morton et al., 2024). Additionally, strain HY8053 was generously provided by the Branzei lab (Psakhye et al., 2019). All the strains listed are isogenic to Y300, a W303 derivative, and they were constructed by tetrad dissection. Standard protocols for transformation, mating, sporulation, and tetrad dissection were used for yeast strain construction. Unless otherwise noted, yeast cells were grown at 30°C in YPD medium or synthetic dropout medium to maintain selection for plasmids. For overexpression of *CDC5*, we cultured cells in a -TRP dropout medium containing 2% raffinose to log phase and induced Cdc5 overproduction by addition of galactose to 2%. For protein tagging, a PCR-based strategy was used (Longtine et al., 1998). For cell cycle synchronization, log phase cells grown at 30°C were arrested in G_1 phase using 5 µg/ml α-factor for 2–3 h. α-factor was added back after G_1 release for 40 min to block the following cell cycle. For HU (Ambeed) arrest, cells in mid-log phase were incubated with 200 mM HU for 2 h. For nocodazole (Sigma-Aldrich) arrest, cells in mid-log phase were treated with 20 µg/ml nocodazole in media containing 1% DMSO for 2 h. Expression of GBP-Cdc5 or GBP-Cdc5^{KD} under the *DDI2* promoter was induced by adding cyanamide to a final concentration of 8 mM. Yeast growth assays were performed by spotting 10-fold serial dilutions of the indicated strains on solid agar plates.

Plasmid construction

The plasmids used in this study are listed in Table S3. Several plasmids were derived from our earlier work, including pUNI10-CDC5-kd, pFH2, and pBAD104 (Hu et al., 2001). Additionally, pSB1252 was kindly provided by the Biggins lab (Akiyoshi et al., 2009), and pET28a-Rpn10 was obtained from the Tomko lab (Nemec et al., 2019). pEGM9 and pEGM10 integrating plasmids were derived from integrating plasmid pEGM5 (Gutierrez-Morton et al., 2024), which is a modified pRS405 plasmid (Sikorski and Hieter, 1989). Briefly, the pEGM9 plasmid (P_{DDI2}-*HA-GBP-CDC5*) was generated by amplifying *CDC5* from

S. cerevisiae genomic DNA before subcloning into pEGM5, replacing *UBC9*. For the pEGM10 plasmid (P_{DDI2}-*HA-GBP-cdc5*^{KD}) construction, *cdc5*^{KD} was amplified using *pUNI10-cdc5*^{KD} as a template and then cloned into pEGM5. Plasmid integration into yeast cells was confirmed by immunoblotting with anti-HA antibody after induction from the *DDI2* promoter by adding cyanamide (Lin et al., 2018). For the construction of the GST-Cdc5 bacterial expression plasmid (pGEX-2T-Cdc5), the ORF of the *CDC5* gene was amplified from *S. cerevisiae* genomic DNA by PCR before subcloning into a pGEX-2T bacterial expression vector. This results in a plasmid that contains the *CDC5* sequence in frame with an N-terminal GST tag. For the construction of the *pET-His-ULP2* bacterial expression plasmid (pET-His-Ulp2), the ORF of the *ULP2* gene was amplified from *S. cerevisiae* genomic DNA by PCR before subcloning into a modified pET-42 bacterial expression vector. This results in a plasmid that contains the *ULP2* sequence in frame with an N-terminal histidine tag. Generation of the *ULP2* S734A point mutation for bacterial expression was performed using the NEB Q5 Site-Directed Mutagenesis kit. The Ulp2 fragment plasmid used for fluorescence polarization assays consisted of an initiator codon and Ulp2 residues 407–767. This fragment was cloned from the full-length Ulp2-coding sequence by PCR using primers to introduce a C-terminal 6xHis tag. Point mutations were introduced via site-directed mutagenesis. The 4×Smt3 expression plasmid was constructed by inserting a custom gBlock (IDT) encoding four tandem Smt3 ORFs with an N-terminal 6×His tag into pET42b. The codons for the two C-terminal glycines of the first three Smt3 copies were replaced with alanine codons, and the terminal glycine codon of the fourth Smt3 copy was replaced with a cysteine codon to allow for fluorophore labeling of the resultant protein. Plasmids were confirmed via sequencing (Sequencing Facility, Florida State University, Tallahassee, FL, USA). All primers, sequences, and plasmid maps are available upon request.

Bacterial expression and purification of GST-Cdc5 and His-Ulp2

Escherichia coli BL21 (DE3) cells were transformed with the *pGEX-2T-CDC5* or *pET-His-ULP2* plasmids and grown overnight at 30°C in LB Miller broth medium with ampicillin (100 µg/ml, final concentration) or kanamycin (50 µg/ml, final concentration), respectively. The overnight cultures were diluted 1:50 in the same medium (with antibiotics) and grown to a density of ∼0.4–0.6 OD at 30°C, at which point the temperature was lowered to 18°C. The expression of recombinant proteins was induced with IPTG at a final concentration of 0.4 mM overnight at 18°C. Following expression, cells were pelleted by centrifugation at 4°C and then resuspended, on ice, in lysis buffer (ice-cold 50 mM Tris, pH 7.5, 150 mM NaCl, 10% glycerol, and 0.25% Triton X-100) supplemented with a cocktail of protease inhibitors. The suspension was sonicated on ice (five to six bursts, 25 s each, with 2-min intervals between sonication bursts to allow cooling). Lysates were cleared by centrifugation at 4°C. Clear bacterial lysates were mixed with immobilized glutathione beads for the purification of GST-Cdc5 or Ni-NTA nickel beads for the purification of His-Ulp2 for a batch method purification. The beads-lysates slurry was incubated with rocking for ∼1 h at 4°C and then centrifuged at 500 × *g* for 1 min at 4°C. The beads were washed five to six times with lysis buffer. Recombinant proteins were then eluted at 4°C from the beads with lysis buffer containing reduced glutathione for GST-Cdc5 or imidazole for His-Ulp2. The eluted proteins were assessed by western blotting analysis, aliquoted, and stored at −80°C until assessed by *in vitro* assays.

In vitro kinase assays

In vitro kinase reactions using purified GST-Cdc5 kinase and His-Ulp2 were performed in kinase buffer (50 mM Tris, pH 7.4, 10 mM MgCl2, 2 mM ATP, 5 mM β-glycerophosphate, 10 mM NaF, and 1 mM DTT) for 1–2 h at 30°C while shaking. Reactions were then stopped by the addition of SDS-PAGE buffer and loaded for separation on a 7% SDS-PAGE gel for western blotting.

Purification of proteins for fluorescence polarization assays

Rpn10 control protein was purified exactly as described previously (Tomko et al., 2015). Ulp2 fragments and 4×Smt3 with the C-terminal glycine of the terminal Smt3 protein changed to a cysteine were expressed in LOBSTR (DE3) cells harboring pRARE2 or pRARE2LysS, respectively. Single colonies were used to inoculate overnight cultures, which were subsequently used to seed large LB cultures containing 50 µg/mL kanamycin and 34 µg/mL chloramphenicol. Cultures were grown at 37°C, 250 rpm to OD_{600} ≈ 1.0, and induced with 0.5 mM IPTG overnight at 16°C. Cells were harvested by centrifugation, resuspended in Tris-NTA buffer (50 mM Tris-Cl, pH 7.5, 500 mM NaCl, 0.2% Triton X-100, 20 mM imidazole, 10% glycerol, and 5 mM β-mercaptoethanol), and either processed immediately or stored at −80°C. Lysates were prepared by high-pressure homogenization using an EmulsiFlex C-5 instrument, and were clarified by centrifugation before incubation with Ni-NTA resin for 30 min at 4°C. The resin was washed extensively with Tris-NTA wash buffer (Tris-NTA buffer instead containing 40 mM imidazole), and proteins were eluted with Tris-NTA cleavage buffer (Tris-NTA buffer instead containing 500 mM imidazole). Proteins were concentrated using 10 kDa MWCO filters (Amicon) and further purified by gel filtration on a hand-packed 120-mL Superose 6-pg column in Ub/DUB buffer (50 mM Tris-Cl, pH 7.5, 100 mM NaCl, 0.1 mM TCEP, and 0.1 mM EDTA). Peak fractions were pooled, concentrated, snap-frozen in liquid nitrogen, and stored at −80°C.

Phosphoserine-S734 Ulp2 expression

For phosphoserine incorporation at position 734 in the Ulp2 fragment, BL95(DE3) *ΔA ΔfabR ΔserB* cells, a gift from Rick Cooley (Zhu et al., 2019), were co-transformed with pRT3204, which encodes amber suppression machinery for phosphoserine incorporation, and pRT3330. Large-scale expression cultures were prepared as described above for other Ulp2 constructs, except they were supplemented with 2 mM O-phospho-*L*-serine at induction. Harvesting, lysis, Ni-NTA purification, and gel filtration were performed exactly as described above. Phosphorylation of the purified protein was evaluated using quercetin phosphoprotein staining (Cong et al., 2014).

Labeling of 4×Smt3 with Oregon Green 488-maleimide

Purified 4×Smt3 (131 µM in 200 µL Ub/DUB buffer lacking TCEP) was incubated with a 2.5-fold molar excess of Oregon Green 488

maleimide (#O6034; Thermo Fisher Scientific) in the dark for 2 h at room temperature. Unreacted dye was quenched with 50 mM DTT for 30 min at room temperature. The labeled protein was separated from the free dye using a Zeba 2-mL spin column (#89882; Thermo Fisher Scientific) pre-equilibrated in Ub/DUB buffer lacking TCEP according to the manufacturer's instructions and then snap-frozen in liquid nitrogen and stored at −80°C.

Fluorescence polarization binding assays

Oregon Green 488–labeled 4×Smt3 was mixed with an equal volume of 2× Ulp2 fragment or Rpn10 control protein, followed by incubation for 1 h at room temperature to allow binding to approach equilibrium. The final concentration of 4×Smt3 was 250 nM, and the concentrations of Ulp2 fragment or Rpn10 consisted of twofold serial dilutions from 80 µM to 1.22 nM. The mixture was then assayed on a BioTek Synergy H1MF microplate reader using the green FP filter set (#804056; Agilent; excitation 485 nm, emission 528 nm, and top read 510 nm). Polarization values were calculated as (A − B)/(A + B), where A and B are the parallel and perpendicular fluorescence intensities, respectively. FP values were plotted vs. concentration, and binding curves were fitted using GraphPad Prism 10 to a one-site binding model to determine binding parameters.

CRISPR-Cas9 genome editing in budding yeast

We used CRISPR-Cas9 to introduce *ulp2* mutations into the yeast genome. CRISPR-Cas9 engineering was performed based on previous work (Laughery and Wyrick, 2019). Briefly, we designed a 20-nucleotide long single-gRNA (sgRNA) matching the target DNA sequence harboring a protospacer-adjacent motif (PAM) within 20 bp's from the site being edited. Synthetic oligonucleotides sequences (IDT) encoding the selected sgRNAs (Table S4) were cloned into pRT2595, a modified pML104 vector that expresses the Cas9 enzyme from *Streptococcus pyogenes* and contains a *URA3* marker, resulting in plasmids pEGM17, pEGM18, and pEGM19. Double-stranded repair templates (donor DNA; Table S4) were synthesized with ∼30–40-bp homology arms and the desired point mutations. To prevent re-cleavage after editing, silent mutations were included to disrupt the PAM sequence. The sgRNA-expressing vector and donor DNA templates were co-transformed into yeast, and the transformants were selected on -URA dropout plates. Colonies were screened for the intended mutations by PCR and confirmed via sequencing (Sequencing Facility, Florida State University, Tallahassee, FL, USA). Positive clones were counterselected on plates containing 5-fluoroorotic acid for the loss of the sgRNA-expressing vector. All sgRNA and donor sequences are listed in Table S4.

Budding index

Cells were taken from culture and fixed with formaldehyde to a final concentration of 3.7%. After sonication, cells were counted and categorized as single cells, small-budded, and large-budded cells based on the existence and size of the daughter cell. A cell was counted as large budded when the diameter of the daughter cell was greater than half of the diameter of the mother cell. The percentage of large-budded cells (100 cells per time point) was plotted.

Fluorescence imaging and analysis

For fluorescence microscopy, collected yeast cells were resuspended in 1 × PBS (pH 7.2) for the examination of fluorescence signals using a BZ-X800 microscope with a 60× objective (NA = 1.40) (Keyence of America). A Z-stack with 11–15 planes of 0.2 µm was acquired for each field and converted to a maximum projection using Keyence BZ-X800 analyzer software. Fluorescence intensity was quantified by measuring signal intensity with the Keyence BZ-X800 imaging analysis software (BZ-H4C). At least 50 cells were counted for each strain and time point. The signal intensity levels are measured in arbitrary units (AU), represented as mean ± SD, and plotted using Graph Pad/Prism software.

Western blotting

Unless otherwise noted, protein samples were prepared using an alkaline method: A cell pellet from 1 mL of cell culture is resuspended in 200 µl 0.1 M NaOH. After 5 min at room temperature, the pellet is collected by centrifugation and resuspended in SDS protein loading buffer. The protein samples were resolved by 10% SDS-PAGE. Nitrocellulose membrane (0.45 µm, PROTRAN) was used. The resources of the antibodies used in this study are listed in Table S1. After ECL (PerkinElmer), western blot membranes were imaged using Bio-Rad ChemiDoc. For visualization of His-Ulp2 and GST-Cdc5, signals were detected using fluorescently labeled secondary antibodies (IRDye 680LT and IRDye 800CW) on a Li-COR Odyssey CLx imager.

Co-IP

Cells were grown in 50 mL YPD at 30°C to OD_{600} = 0.75. For the treatment with proteasome inhibitor MG-132 (Millipore), cells were first incubated with 0.1% L-proline and 0.003% SDS for 3 h (Chuang et al., 2016). Then, MG-132 (50 µM) was added for 30 min before harvesting. Harvested cells were resuspended in 700 µl RIPA buffer (50 mM Tris-HCl, pH 7.5, 150 mM NaCl, 5 mM EDTA, and 0.05% TWEEN-20) supplemented with protease inhibitor cocktail and 20 mM N-ethylmaleimide. For the co-IP experiments to examine the interaction between Ulp2 and SUMO conjugates, phosphatase inhibitors were added to the lysates (10 mM β-glycerophosphate, 10 mM NaF, and 10 mM NaV). Samples were then frozen by slowly dripping them into liquid nitrogen to form frozen droplets called "popcorn." These popcorns were crushed using a freezer mill (Cole-Parmer). Once crushed, samples were allowed to thaw on ice. Then, samples were centrifuged at 1,800 *g* for 20 min at 4°C. Supernatant was collected and centrifuged again at 20,000 *g* for 20 min at 4°C. Input sample was collected, and the remaining cell extracts were incubated with anti-FLAG beads (Sigma-Aldrich) for 4 h at 4°C. After incubation, the beads were collected by centrifugation and washed three times with buffer. After removal of buffer, 1× SDS protein loading buffer was added, and the protein samples were incubated for 10 min at 65°C before immunoblotting.

Protein level quantification and statistical analysis

To quantify protein levels from western blots, we used ImageJ to acquire the intensity of each protein band from western blotting images. Then, the protein levels were normalized by determining the ratio to loading control, Pgk1. For quantification of the

Ulp2 phosphorylation band shift, a straight line of consistent length was drawn through the Ulp2 protein bands for the indicated time points and the intensity of protein signal (AU) across the line was plotted. All statistical analyses and graph preparations were done using Graph Pad/Prism software. The mean values were calculated and appeared with corresponding SDs in bar graphs. We performed unpaired *t* tests, one-way ANOVAs, or two-way ANOVAs, and the significance was corrected for multiple comparisons using Tukey's correction to generate a significance of $^{*}p < 0.05$, $^{**}p < 0.01$, $^{***}p < 0.001$, or $^{****}p < 0.0001$ and is denoted as such.

Online supplemental material

Fig. S1 shows that Ulp2 phosphorylation during the cell cycle is delayed in *ulp2*^{S734A} mutant. Fig. S2 shows that accumulation of polySUMO conjugates is impaired in *cdc5-2* or phosphodeficient *ulp2*^{S734A} cells. Fig. S3 shows that deletion of *RTS1* causes delayed Ulp2 dephosphorylation. Fig. S4 shows validation of reagents used for binding analyses between Ulp2 and 4×Smt3. Table S1 shows key resources used in this study. Table S2 shows relevant genotypes and sources of the yeast strains used in this study. Table S3 shows plasmids used in this study. Table S4 shows DNA oligonucleotides used in this study for CRISPR mutagenesis.

Data availability

Data are available in the article itself and its supplemental material.

Acknowledgments

We are grateful to the yeast community at Florida State University for reagents and helpful suggestions. We thank Anthony Woo (The Lawrenceville School, Lawrenceville, NJ, USA) for his help in the construction of *GBP-CDC5* plasmids and relevant yeast strains. We thank Dr. Sue Biggins (Fred Hutchinson Cancer Center, Seattle, WA, USA) for providing the *FIN1-GFP* (pSB1252) plasmid and Dr. Cindy Vied (Florida State University, Tallahassee, FL, USA) for performing the mass spectrometry analysis. We are grateful to Dr. Terra Bradley (Florida State University, Tallahassee, FL, USA) for reading and improving English in the manuscript.

This work was supported by R01GM151447 from National Institutes of Health to Y. Wang and R01GM118600 to R.J. Tomko.

Author contributions: Emily Gutierrez-Morton: conceptualization, data curation, formal analysis, investigation, methodology, resources, supervision, validation, visualization, and writing—original draft, review, and editing. Raed Rizkallah: conceptualization, data curation, formal analysis, investigation, methodology, validation, and writing—original draft. Tomiwa Lawal: data curation, formal analysis, investigation, and methodology. Marie-Helene Kabbaj: data curation, investigation, and methodology. Sophia L. Owutey: data curation, formal analysis, and investigation. Robert J. Tomko Jr: Conceptualization, formal analysis, funding acquisition, methodology, resources, supervision, and writing—original draft, review, and editing. Yanchang Wang: conceptualization, data curation, formal analysis, funding acquisition, investigation, methodology, project administration, resources, supervision, validation, visualization, and writing—review and editing.

Disclosures: The authors declare no competing interests exist.

Submitted: 17 January 2025
Revised: 12 September 2025
Accepted: 5 January 2026

References

Akiyoshi, B., C.R. Nelson, J.A. Ranish, and S. Biggins. 2009. Quantitative proteomic analysis of purified yeast kinetochores identifies a PP1 regulatory subunit. *Genes Dev.* 23:2887–2899. https://doi.org/10.1101/gad.1865909

Albuquerque, C.P., G. Wang, N.S. Lee, R.D. Kolodner, C.D. Putnam, and H. Zhou. 2013. Distinct SUMO ligases cooperate with Esc2 and Slx5 to suppress duplication-mediated genome rearrangements. *PLoS Genet.* 9: e1003670. https://doi.org/10.1371/journal.pgen.1003670

Alexandru, G., F. Uhlmann, K. Mechtler, M.A. Poupart, and K. Nasmyth. 2001. Phosphorylation of the cohesin subunit Scc1 by Polo/Cdc5 kinase regulates sister chromatid separation in yeast. *Cell.* 105:459–472. https://doi.org/10.1016/s0092-8674(01)00362-2

Baldwin, M.L., J.A. Julius, X. Tang, Y. Wang, and J. Bachant. 2009. The yeast SUMO isopeptidase Smt4/Ulp2 and the polo kinase Cdc5 act in an opposing fashion to regulate sumoylation in mitosis and cohesion at centromeres. *Cell Cycle.* 8:3406–3419. https://doi.org/10.4161/cc.8.20.9911

Bartholomew, C.R., S.H. Woo, Y.S. Chung, C. Jones, and C.F. Hardy. 2001. Cdc5 interacts with the Wee1 kinase in budding yeast. *Mol. Cell Biol.* 21: 4949–4959. https://doi.org/10.1128/MCB.21.15.4949-4959.2001

Bergink, S., T. Ammon, M. Kern, L. Schermelleh, H. Leonhardt, and S. Jentsch. 2013. Role of Cdc48/p97 as a SUMO-targeted segregase curbing Rad51-Rad52 interaction. *Nat. Cell Biol.* 15:526–532. https://doi.org/10.1038/ncb2729

Bokros, M., C. Gravenmier, F. Jin, D. Richmond, and Y. Wang. 2016. Fin1-PP1 helps clear spindle assembly checkpoint protein Bub1 from kinetochores in anaphase. *Cell Rep.* 14:1074–1085. https://doi.org/10.1016/j.celrep.2016.01.007

Bremmer, S.C., H. Hall, J.S. Martinez, C.L. Eissler, T.H. Hinrichsen, S. Rossie, L.L. Parker, M.C. Hall, and H. Charbonneau. 2012. Cdc14 phosphatases preferentially dephosphorylate a subset of cyclin-dependent kinase (Cdk) sites containing phosphoserine. *J. Biol. Chem.* 287:1662–1669. https://doi.org/10.1074/jbc.M111.281105

Bylebyl, G.R., I. Belichenko, and E.S. Johnson. 2003. The SUMO isopeptidase Ulp2 prevents accumulation of SUMO chains in yeast. *J. Biol. Chem.* 278: 44113–44120. https://doi.org/10.1074/jbc.M308357200

Capili, A.D., and C.D. Lima. 2007. Structure and analysis of a complex between SUMO and Ubc9 illustrates features of a conserved E2-Ubl interaction. *J. Mol. Biol.* 369:608–618. https://doi.org/10.1016/j.jmb.2007.04.006

Charles, J.F., S.L. Jaspersen, R.L. Tinker-Kulberg, L. Hwang, A. Szidon, and D.O. Morgan. 1998. The polo-related kinase Cdc5 activates and is destroyed by the mitotic cyclin destruction machinery in *S. cerevisiae*. *Curr. Biol.* 8:497–507. https://doi.org/10.1016/s0960-9822(98)70201-5

Chen, M., W. Zhang, Y. Gou, D. Xu, Y. Wei, D. Liu, C. Han, X. Huang, C. Li, W. Ning, et al. 2023. GPS 6.0: An updated server for prediction of kinase-specific phosphorylation sites in proteins. *Nucleic Acids Res.* 51: W243–w250. https://doi.org/10.1093/nar/gkad383

Chen, Y.C., and M. Weinreich. 2010. Dbf4 regulates the Cdc5 polo-like kinase through a distinct non-canonical binding interaction. *J. Biol. Chem.* 285: 41244–41254. https://doi.org/10.1074/jbc.M110.155242

Chuang, K.H., F. Liang, R. Higgins, and Y. Wang. 2016. Ubiquilin/Dsk2 promotes inclusion body formation and vacuole (lysosome)-mediated disposal of mutated huntingtin. *Mol. Biol. Cell.* 27:2025–2036. https://doi.org/10.1091/mbc.E16-01-0026

Cong, W., J. Shen, Y. Xuan, X. Zhu, M. Ni, Z. Zhu, G. Hong, X. Lu, and L. Jin. 2014. A simple, rapid and low-cost staining method for gel-electrophoresis separated phosphoproteins via the fluorescent purpurin dye. *Analyst.* 139: 6104–6108. https://doi.org/10.1039/c4an01334d

D'Ambrosio, L.M., and B.D. Lavoie. 2014. Pds5 prevents the PolySUMO-dependent separation of sister chromatids. *Curr. Biol.* 24:361–371. https://doi.org/10.1016/j.cub.2013.12.038

de Albuquerque, C.P., J. Liang, N.J. Gaut, and H. Zhou. 2016. Molecular circuitry of the SUMO (small ubiquitin-like modifier) pathway in controlling sumoylation homeostasis and suppressing genome rearrangements. *J. Biol. Chem.* 291:8825–8835. https://doi.org/10.1074/jbc.M116.716399

de Albuquerque, C.P., R.T. Suhandynata, C.R. Carlson, W.T. Yuan, and H. Zhou. 2018. Binding to small ubiquitin-like modifier and the nucleolar protein Csm1 regulates substrate specificity of the Ulp2 protease. *J. Biol. Chem.* 293:12105–12119. https://doi.org/10.1074/jbc.RA118.003022

Dyson, H.J., and P.E. Wright. 2005. Intrinsically unstructured proteins and their functions. *Nat. Rev. Mol. Cell Biol.* 6:197–208. https://doi.org/10.1038/nrm1589

Eckhoff, J., and R.J. Dohmen. 2015. In vitro studies reveal a sequential mode of chain processing by the yeast SUMO (small ubiquitin-related modifier)-specific protease Ulp2. *J. Biol. Chem.* 290:12268–12281. https://doi.org/10.1074/jbc.M114.622217

Folger, A., E. Gutierrez-Morton, M.H. Kabbaj, M.T. Campbell, G. Morton, T.L. Megraw, and Y. Wang. 2025. Regulation of misfolded protein aggregation and degradation by SUMOylation in budding yeast. *Mol. Biol. Cell.* 36:ar77. https://doi.org/10.1091/mbc.E24-12-0540

Folger, A., and Y. Wang. 2021. The cytotoxicity and clearance of mutant huntingtin and other misfolded proteins. *Cells*. 10:2835. https://doi.org/10.3390/cells10112835

Geiss-Friedlander, R., and F. Melchior. 2007. Concepts in sumoylation: A decade on. *Nat. Rev. Mol. Cell Biol.* 8:947–956. https://doi.org/10.1038/nrm2293

Guerra de Souza, A.C., R.D. Prediger, and H. Cimarosti. 2016. SUMO-regulated mitochondrial function in Parkinson's disease. *J. Neurochem.* 137:673–686. https://doi.org/10.1111/jnc.13599

Gutierrez-Morton, E., C. Haluska, L. Collins, R. Rizkallah, R.J. Tomko Jr, and Y. Wang. 2024. The polySUMOylation axis promotes nucleolar release of Tof2 for mitotic exit. *Cell Rep.* 43:114492. https://doi.org/10.1016/j.celrep.2024.114492

Gutierrez-Morton, E., and Y. Wang. 2024. The role of SUMOylation in biomolecular condensate dynamics and protein localization. *Cell Insight*. 3:100199. https://doi.org/10.1016/j.cellin.2024.100199

Han, Z.J., Y.H. Feng, B.H. Gu, Y.M. Li, and H. Chen. 2018. The post-translational modification, SUMOylation, and cancer (Review). *Int. J. Oncol.* 52:1081–1094.https://doi.org/10.3892/ijo.2018.4280

Hardy, C.F., and A. Pautz. 1996. A novel role for Cdc5p in DNA replication. *Mol. Cell Biol.* 16:6775–6782. https://doi.org/10.1128/MCB.16.12.6775

Holt, L.J., B.B. Tuch, J. Villén, A.D. Johnson, S.P. Gygi, and D.O. Morgan. 2009. Global analysis of Cdk1 substrate phosphorylation sites provides insights into evolution. *Science*. 325:1682–1686. https://doi.org/10.1126/science.1172867

Hu, F., Y. Wang, D. Liu, Y. Li, J. Qin, and S.J. Elledge. 2001. Regulation of the Bub2/Bfa1 GAP complex by Cdc5 and cell cycle checkpoints. *Cell*. 107:655–665. https://doi.org/10.1016/s0092-8674(01)00580-3

Jin, F., M. Bokros, and Y. Wang. 2017. Premature silencing of the spindle assembly checkpoint is prevented by the Bub1-H2A-Sgo1-PP2A axis in *Saccharomyces cerevisiae*. *Genetics*. 205:1169–1178. https://doi.org/10.1534/genetics.116.195727

Johnson, E.S., and A.A. Gupta. 2001. An E3-like factor that promotes SUMO conjugation to the yeast septins. *Cell*. 106:735–744. https://doi.org/10.1016/s0092-8674(01)00491-3

Keiten-Schmitz, J., K. Schunck, and S. Muller. 2019. SUMO chains rule on chromatin occupancy. *Front. Cell Dev. Biol.* 7:343. https://doi.org/10.3389/fcell.2019.00343

Kerscher, O., R. Felberbaum, and M. Hochstrasser. 2006. Modification of proteins by ubiquitin and ubiquitin-like proteins. *Annu. Rev. Cell Dev. Biol.* 22:159–180. https://doi.org/10.1146/annurev.cellbio.22.010605.093503

Kitada, K., A.L. Johnson, L.H. Johnston, and A. Sugino. 1993. A multicopy suppressor gene of the *Saccharomyces cerevisiae* G1 cell cycle mutant gene dbf4 encodes a protein kinase and is identified as CDC5. *Mol. Cell Biol.* 13:4445–4457. https://doi.org/10.1128/mcb.13.7.4445-4457.1993

Kramarz, K., K. Schirmeisen, V. Boucherit, A. Ait Saada, C. Lovo, B. Palancade, C. Freudenreich, and S.A.E. Lambert. 2020. The nuclear pore primes recombination-dependent DNA synthesis at arrested forks by promoting SUMO removal. *Nat. Commun.* 11:5643. https://doi.org/10.1038/s41467-020-19516-z

Kroetz, M.B., D. Su, and M. Hochstrasser. 2009. Essential role of nuclear localization for yeast Ulp2 SUMO protease function. *Mol. Biol. Cell*. 20:2196–2206. https://doi.org/10.1091/mbc.e08-10-1090

Laughery, M.F., and J.J. Wyrick. 2019. Simple CRISPR-Cas9 genome editing in *Saccharomyces cerevisiae*. *Curr. Protoc. Mol. Biol.* 129:e110. https://doi.org/10.1002/cpmb.110

Li, S.J., and M. Hochstrasser. 2000. The yeast ULP2 (SMT4) gene encodes a novel protease specific for the ubiquitin-like Smt3 protein. *Mol. Cell Biol.* 20:2367–2377. https://doi.org/10.1128/MCB.20.7.2367-2377.2000

Li, S.J., and M. Hochstrasser. 2003. The Ulp1 SUMO isopeptidase: Distinct domains required for viability, nuclear envelope localization, and substrate specificity. *J. Cell Biol.* 160:1069–1081. https://doi.org/10.1083/jcb.200212052

Li, Y., A. De Bolòs, V. Amador, and D. Reverter. 2022. Structural basis for the SUMO2 isoform specificity of SENP7. *J. Mol. Biol.* 434:167875. https://doi.org/10.1016/j.jmb.2022.167875

Liang, F., F. Jin, H. Liu, and Y. Wang. 2009. The molecular function of the yeast polo-like kinase Cdc5 in Cdc14 release during early anaphase. *Mol. Biol. Cell*. 20:3671–3679. https://doi.org/10.1091/mbc.e08-10-1049

Liang, F., and Y. Wang. 2007. DNA damage checkpoints inhibit mitotic exit by two different mechanisms. *Mol. Cell Biol.* 27:5067–5078. https://doi.org/10.1128/MCB.00095-07

Liang, J., N. Singh, C.R. Carlson, C.P. Albuquerque, K.D. Corbett, and H. Zhou. 2017. Recruitment of a SUMO isopeptidase to rDNA stabilizes silencing complexes by opposing SUMO targeted ubiquitin ligase activity. *Genes Dev.* 31:802–815. https://doi.org/10.1101/gad.296145.117

Lima, C.D., and D. Reverter. 2008. Structure of the human SENP7 catalytic domain and poly-SUMO deconjugation activities for SENP6 and SENP7. *J. Biol. Chem.* 283:32045–32055. https://doi.org/10.1074/jbc.M805655200

Lin, A., C. Zeng, Q. Wang, W. Zhang, M. Li, M. Hanna, and W. Xiao. 2018. Utilization of a strongly inducible DDI2 promoter to control gene expression in *Saccharomyces cerevisiae*. *Front. Microbiol.* 9:2736. https://doi.org/10.3389/fmicb.2018.02736

Linding, R., L.J. Jensen, F. Diella, P. Bork, T.J. Gibson, and R.B. Russell. 2003. Protein disorder prediction: Implications for structural proteomics. *Structure*. 11:1453–1459. https://doi.org/10.1016/j.str.2003.10.002

Longtine, M.S., A. McKenzie 3rd, D.J. Demarini, N.G. Shah, A. Wach, A. Brachat, P. Philippsen, and J.R. Pringle. 1998. Additional modules for versatile and economical PCR-based gene deletion and modification in *Saccharomyces cerevisiae*. *Yeast*. 14:953–961. https://doi.org/10.1002/(SICI)1097-0061(199807)14:10<953::AID-YEA293>3.0.CO;2-U

Miller, C.T., C. Gabrielse, Y.C. Chen, and M. Weinreich. 2009. Cdc7p-Dbf4p regulates mitotic exit by inhibiting polo kinase. *PLoS Genet.* 5:e1000498. https://doi.org/10.1371/journal.pgen.1000498

Mishra, P.K., G. Olafsson, L. Boeckmann, T.J. Westlake, Z.M. Jowhar, L.E. Dittman, R.E. Baker, D. D'Amours, P.H. Thorpe, and M.A. Basrai. 2019. Cell cycle-dependent association of polo kinase Cdc5 with CENP-A contributes to faithful chromosome segregation in budding yeast. *Mol. Biol. Cell*. 30:1020–1036. https://doi.org/10.1091/mbc.E18-09-0584

Mossessova, E., and C.D. Lima. 2000. Ulp1-SUMO crystal structure and genetic analysis reveal conserved interactions and a regulatory element essential for cell growth in yeast. *Mol. Cell*. 5:865–876. https://doi.org/10.1016/s1097-2765(00)80326-3

Mullen, J.R., and S.J. Brill. 2008. Activation of the Slx5-Slx8 ubiquitin ligase by poly-small ubiquitin-like modifier conjugates. *J. Biol. Chem.* 283:19912–19921. https://doi.org/10.1074/jbc.M802690200

Nakajima, H., F. Toyoshima-Morimoto, E. Taniguchi, and E. Nishida. 2003. Identification of a consensus motif for Plk (polo-like kinase) phosphorylation reveals Myt1 as a Plk1 substrate. *J. Biol. Chem.* 278:25277–25280. https://doi.org/10.1074/jbc.C300126200

Nemec, A.A., A.K. Peterson, J.L. Warnock, R.G. Reed, and R.J. Tomko Jr. 2019. An allosteric interaction network promotes conformation state-dependent eviction of the Nas6 assembly chaperone from nascent 26S proteasomes. *Cell Rep.* 26:483–495.e5. https://doi.org/10.1016/j.celrep.2018.12.042

Ohkuni, K., Y. Takahashi, A. Fulp, J. Lawrimore, W.C. Au, N. Pasupala, R. Levy-Myers, J. Warren, A. Strunnikov, R.E. Baker, et al. 2016. SUMO-targeted ubiquitin ligase (STUbL) Slx5 regulates proteolysis of centromeric histone H3 variant Cse4 and prevents its mislocalization to euchromatin. *Mol. Biol. Cell*. 27:1500–1510. https://doi.org/10.1091/mbc.E15-12-0827

Panse, V.G., B. Kuster, T. Gerstberger, and E. Hurt. 2003. Unconventional tethering of Ulp1 to the transport channel of the nuclear pore complex by karyopherins. *Nat. Cell Biol.* 5:21–27. https://doi.org/10.1038/ncb893

Princz, A., and N. Tavernarakis. 2020. SUMOylation in neurodegenerative diseases. *Gerontology*. 66:122–130. https://doi.org/10.1159/000502142

Princz, L.N., P. Wild, J. Bittmann, F.J. Aguado, M.G. Blanco, J. Matos, and B. Pfander. 2017. Dbf4-dependent kinase and the Rtt107 scaffold promote Mus81-Mms4 resolvase activation during mitosis. *EMBO J.* 36:664–678. https://doi.org/10.15252/embj.201694831

Prudden, J., S. Pebernard, G. Raffa, D.A. Slavin, J.J. Perry, J.A. Tainer, C.H. McGowan, and M.N. Boddy. 2007. SUMO-targeted ubiquitin ligases in genome stability. *EMBO J.* 26:4089–4101. https://doi.org/10.1038/sj.emboj.7601838

Psakhye, I., and D. Branzei. 2021. SMC complexes are guarded by the SUMO protease Ulp2 against SUMO-chain-mediated turnover. *Cell Rep.* 36:109485. https://doi.org/10.1016/j.celrep.2021.109485

Psakhye, I., F. Castellucci, and D. Branzei. 2019. SUMO-chain-regulated proteasomal degradation timing exemplified in DNA replication initiation. *Mol. Cell.* 76:632–645.e6. https://doi.org/10.1016/j.molcel.2019.08.003

Quan, Y., S.M. Hinshaw, P.C. Wang, S.C. Harrison, and H. Zhou. 2021. Ctf3/CENP-I provides a docking site for the desumoylase Ulp2 at the kinetochore. *J. Cell Biol.* 220:e202012149. https://doi.org/10.1083/jcb.202012149

Queralt, E., C. Lehane, B. Novak, and F. Uhlmann. 2006. Downregulation of PP2A(Cdc55) phosphatase by separase initiates mitotic exit in budding yeast. *Cell.* 125:719–732. https://doi.org/10.1016/j.cell.2006.03.038

Rothbauer, U., K. Zolghadr, S. Muyldermans, A. Schepers, M.C. Cardoso, and H. Leonhardt. 2008. A versatile nanotrap for biochemical and functional studies with fluorescent fusion proteins. *Mol. Cell Proteomics.* 7:282–289. https://doi.org/10.1074/mcp.M700342-MCP200

Rothbauer, U., K. Zolghadr, S. Tillib, D. Nowak, L. Schermelleh, A. Gahl, N. Backmann, K. Conrath, S. Muyldermans, M.C. Cardoso, and H. Leonhardt. 2006. Targeting and tracing antigens in live cells with fluorescent nanobodies. *Nat. Methods.* 3:887–889. https://doi.org/10.1038/nmeth953

Ryu, H.Y., N.R. Wilson, S. Mehta, S.S. Hwang, and M. Hochstrasser. 2016. Loss of the SUMO protease Ulp2 triggers a specific multichromosome aneuploidy. *Genes Dev.* 30:1881–1894. https://doi.org/10.1101/gad.282194.116

Shou, W., R. Azzam, S.L. Chen, M.J. Huddleston, C. Baskerville, H. Charbonneau, R.S. Annan, S.A. Carr, and R.J. Deshaies. 2002. Cdc5 influences phosphorylation of Net1 and disassembly of the RENT complex. *BMC Mol. Biol.* 3:3. https://doi.org/10.1186/1471-2199-3-3

Shou, W., J.H. Seol, A. Shevchenko, C. Baskerville, D. Moazed, Z.W. Chen, J. Jang, A. Shevchenko, H. Charbonneau, and R.J. Deshaies. 1999. Exit from mitosis is triggered by Tem1-dependent release of the protein phosphatase Cdc14 from nucleolar RENT complex. *Cell.* 97:233–244. https://doi.org/10.1016/s0092-8674(00)80733-3

Sikorski, R.S., and P. Hieter. 1989. A system of shuttle vectors and yeast host strains designed for efficient manipulation of DNA in *Saccharomyces cerevisiae*. *Genetics.* 122:19–27. https://doi.org/10.1093/genetics/122.1.19

Snead, J.L., M. Sullivan, D.M. Lowery, M.S. Cohen, C. Zhang, D.H. Randle, J. Taunton, M.B. Yaffe, D.O. Morgan, and K.M. Shokat. 2007. A coupled chemical-genetic and bioinformatic approach to polo-like kinase pathway exploration. *Chem. Biol.* 14:1261–1272. https://doi.org/10.1016/j.chembiol.2007.09.011

Sneddon, A.A., P.T. Cohen, and M.J. Stark. 1990. *Saccharomyces cerevisiae* protein phosphatase 2A performs an essential cellular function and is encoded by two genes. *EMBO J.* 9:4339–4346. https://doi.org/10.1002/j.1460-2075.1990.tb07883.x

Song, J., L.K. Durrin, T.A. Wilkinson, T.G. Krontiris, and Y. Chen. 2004. Identification of a SUMO-binding motif that recognizes SUMO-modified proteins. *Proc. Natl. Acad. Sci. USA.* 101:14373–14378. https://doi.org/10.1073/pnas.0403498101

Srikumar, T., M.C. Lewicki, and B. Raught. 2013. A global *S. cerevisiae* small ubiquitin-related modifier (SUMO) system interactome. *Mol. Syst. Biol.* 9:668. https://doi.org/10.1038/msb.2013.23

St-Pierre, J., M. Douziech, F. Bazile, M. Pascariu, E. Bonneil, V. Sauve, H. Ratsima, and D. D'Amours. 2009. Polo kinase regulates mitotic chromosome condensation by hyperactivation of condensin DNA supercoiling activity. *Mol. Cell.* 34:416–426. https://doi.org/10.1016/j.molcel.2009.04.013

Suhandynata, R.T., Y. Quan, Y. Yang, W.T. Yuan, C.P. Albuquerque, and H. Zhou. 2019. Recruitment of the Ulp2 protease to the inner kinetochore prevents its hyper-sumoylation to ensure accurate chromosome segregation. *PLoS Genet.* 15:e1008477. https://doi.org/10.1371/journal.pgen.1008477

Surana, U., A. Amon, C. Dowzer, J. McGrew, B. Byers, and K. Nasmyth. 1993. Destruction of the CDC28/CLB mitotic kinase is not required for the metaphase to anaphase transition in budding yeast. *EMBO J.* 12:1969–1978. https://doi.org/10.1002/j.1460-2075.1993.tb05846.x

Takahashi, Y., T. Kahyo, E.A. Toh, H. Yasuda, and Y. Kikuchi. 2001. Yeast Ulli1/Siz1 is a novel SUMO1/Smt3 ligase for septin components and functions as an adaptor between conjugating enzyme and substrates. *J. Biol. Chem.* 276:48973–48977. https://doi.org/10.1074/jbc.M109295200

Tomko, R.J., Jr, D.W. Taylor, Z.A. Chen, H.W. Wang, J. Rappsilber, and M. Hochstrasser. 2015. A single alpha helix drives extensive remodeling of the proteasome lid and completion of regulatory particle assembly. *Cell.* 163:432–444. https://doi.org/10.1016/j.cell.2015.09.022

Ubersax, J.A., E.L. Woodbury, P.N. Quang, M. Paraz, J.D. Blethrow, K. Shah, K.M. Shokat, and D.O. Morgan. 2003. Targets of the cyclin-dependent kinase Cdk1. *Nature.* 425:859–864. https://doi.org/10.1038/nature02062

Visintin, R., E.S. Hwang, and A. Amon. 1999. Cfi1 prevents premature exit from mitosis by anchoring Cdc14 phosphatase in the nucleolus. *Nature.* 398:818–823. https://doi.org/10.1038/19775

Waizenegger, A., M. Urulangodi, C.P. Lehmann, T.A.C. Reyes, I. Saugar, J.A. Tercero, B. Szakal, and D. Branzei. 2020. Mus81-Mms4 endonuclease is an Esc2-STUbL-Cullin8 mitotic substrate impacting on genome integrity. *Nat. Commun.* 11:5746. https://doi.org/10.1038/s41467-020-19503-4

Wang, Y., and T.Y. Ng. 2006. Phosphatase 2A negatively regulates mitotic exit in *Saccharomyces cerevisiae*. *Mol. Biol. Cell.* 17:80–89. https://doi.org/10.1091/mbc.e04-12-1109

Wang, Y., T. Shirogane, D. Liu, J.W. Harper, and S.J. Elledge. 2003. Exit from exit: Resetting the cell cycle through Amn1 inhibition of G protein signaling. *Cell.* 112:697–709. https://doi.org/10.1016/s0092-8674(03)00121-1

Waples, W.G., C. Chahwan, M. Ciechonska, and B.D. Lavoie. 2009. Putting the brake on FEAR: Tof2 promotes the biphasic release of Cdc14 phosphatase during mitotic exit. *Mol. Biol. Cell.* 20:245–255. https://doi.org/10.1091/mbc.e08-08-0879

Wohlschlegel, J.A., E.S. Johnson, S.I. Reed, and J.R. Yates 3rd. 2004. Global analysis of protein sumoylation in *Saccharomyces cerevisiae*. *J. Biol. Chem.* 279:45662–45668. https://doi.org/10.1074/jbc.M409203200

Wu, N., X. Kong, Z. Ji, W. Zeng, P.R. Potts, K. Yokomori, and H. Yu. 2012. Scc1 sumoylation by Mms21 promotes sister chromatid recombination through counteracting Wapl. *Genes Dev.* 26:1473–1485. https://doi.org/10.1101/gad.193615.112

Xie, M., J. Yu, S. Ge, J. Huang, and X. Fan. 2020. SUMOylation homeostasis in tumorigenesis. *Cancer Lett.* 469:301–309. https://doi.org/10.1016/j.canlet.2019.11.004

Xie, Y., O. Kerscher, M.B. Kroetz, H.F. McConchie, P. Sung, and M. Hochstrasser. 2007. The yeast Hex3.Slx8 heterodimer is a ubiquitin ligase stimulated by substrate sumoylation. *J. Biol. Chem.* 282:34176–34184. https://doi.org/10.1074/jbc.M706025200

Yellman, C.M., and D.J. Burke. 2006. The role of Cdc55 in the spindle checkpoint is through regulation of mitotic exit in *Saccharomyces cerevisiae*. *Mol. Biol. Cell.* 17:658–666. https://doi.org/10.1091/mbc.e05-04-0336

Zhao, X., and G. Blobel. 2005. A SUMO ligase is part of a nuclear multiprotein complex that affects DNA repair and chromosomal organization. *Proc. Natl. Acad. Sci. USA.* 102:4777–4782. https://doi.org/10.1073/pnas.0500537102

Zhu, P., P.R. Gafken, R.A. Mehl, and R.B. Cooley. 2019. A highly versatile expression system for the production of multiply phosphorylated proteins. *ACS Chem. Biol.* 14:1564–1572. https://doi.org/10.1021/acschembio.9b00307

Supplemental material

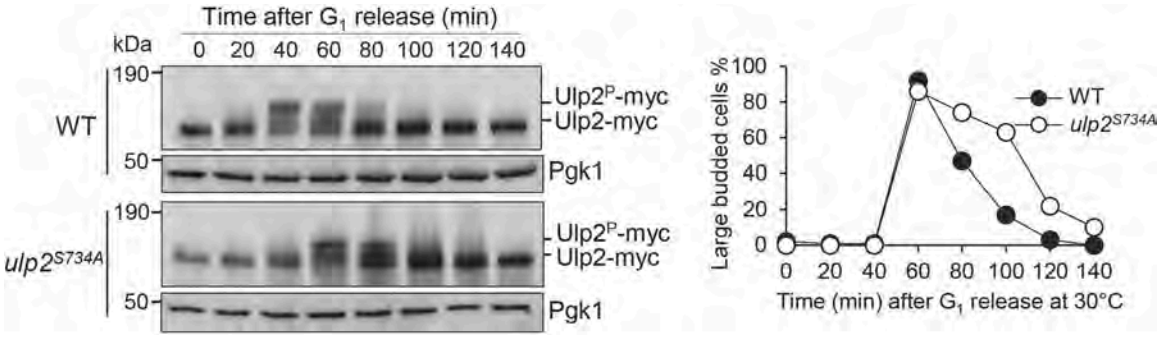

Figure S1. **Ulp2 phosphorylation during the cell cycle is delayed in *ulp2^{S734A}* mutant.** G_1-arrested *ULP2-13myc* (YCH25) and *ulp2^{S734A}-13myc* (EGM51) cells were released into the cell cycle at 30°C. Cells were collected every 20 min for western blotting with anti-myc antibody and budding index. Pgk1, loading control.

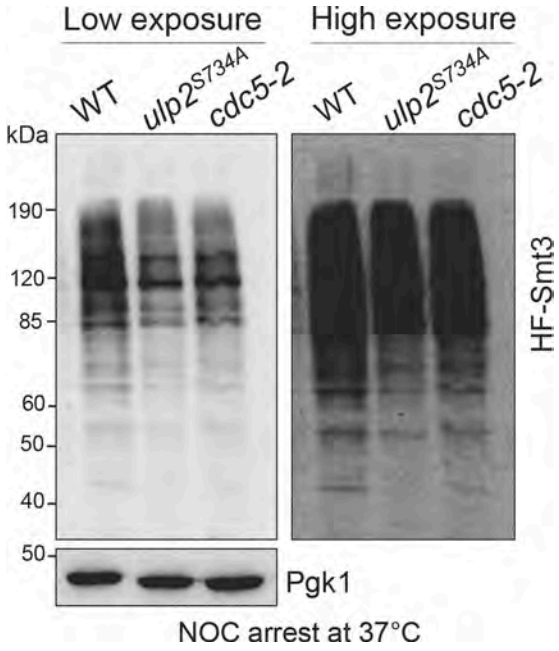

Figure S2. **Accumulation of polySUMO conjugates is impaired in *cdc5-2* or phosphodeficient *ulp2^{S734A}* cells.** WT (4160-1-2), *ulp2^{S734A}-13myc* (4903-3-1), and *cdc5-2* (4161-3-2) cells with HF-Smt3 were arrested in nocodazole (NOC) at 37°C before preparing protein extracts for western blotting with anti-FLAG antibody to detect total protein SUMOylation. Pgk1, loading control. Source data are available for this figure: SourceData FS2.

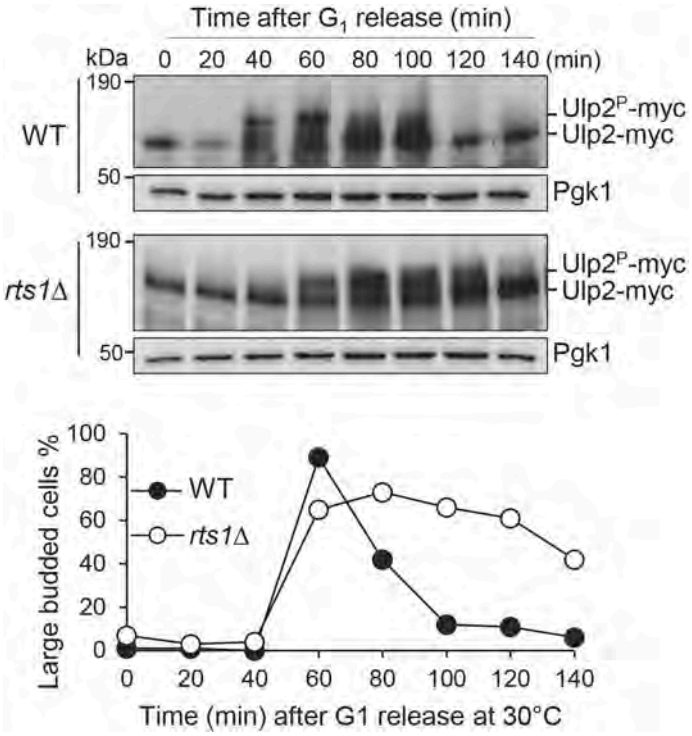

Figure S3. **Deletion of *RTS1* causes delayed Ulp2 dephosphorylation.** G_1-arrested *ULP2-13myc* (YCH25) and *rts1Δ ULP2-13myc* (4786-2-1) cells were released into the cell cycle at 30°C after G_1 arrest. Cells were collected every 20 min for western blotting with anti-myc antibody and budding index. Pgk1, loading control. Source data are available for this figure: SourceData FS3.

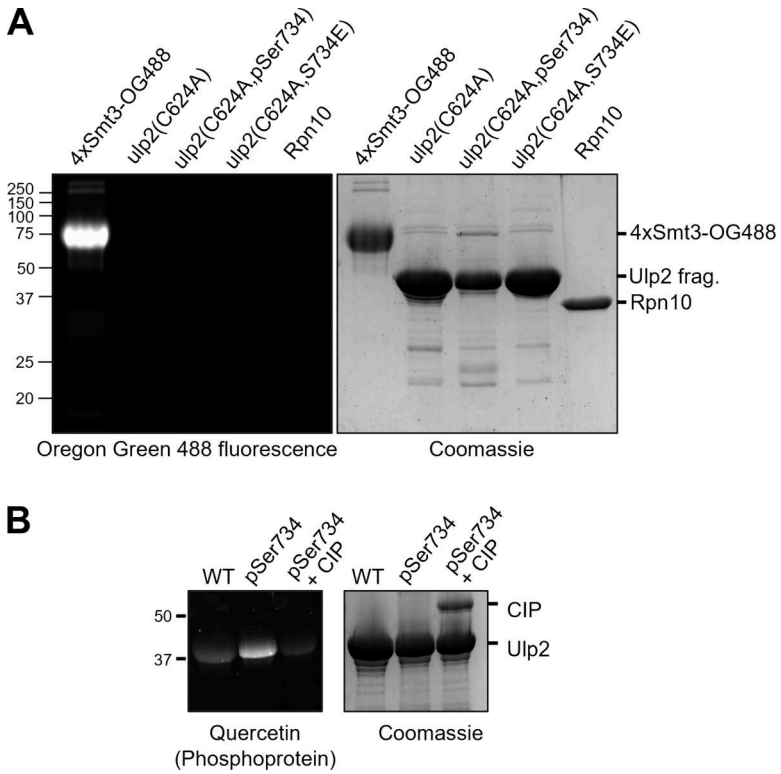

Figure S4. **Validation of reagents used for binding analyses between Ulp2 and 4×Smt3. (A)** SDS-PAGE analysis of the indicated proteins. **(B)** Quercetin phosphoprotein staining of WT Ulp2 fragment (left lane) and pSer734-Ulp2 prior to or after treatment with calf-intestinal phosphatase for 1 h (middle and right lanes, respectively). Source data are available for this figure: SourceData FS4.

Provided online are Table S1, Table S2, Table S3, and Table S4. Table S1 shows key resources used in this study. Table S2 shows relevant genotypes and sources of the yeast strains used in this study. Table S3 shows plasmids used in this study. Table S4 shows DNA oligonucleotides used in this study for CRISPR mutagenesis.